Nuclear Science and Engineering

ISSN: (Print) (Online) Journal homepage: https://www.tandfonline.com/loi/unse20

The HighNESS Project at the European Spallation Source: Current Status and Future Perspectives

V. Santoro, K. H. Andersen, P. Bentley, M. Bernasconi, M. Bertelsen, Y. Beßler, A. Bianchi, T. Brys, D. Campi, A. Chambon, V. Czamler, D. D. Di Julio, E. Dian, K. Dunne, M. J. Ferreira, P. Fierlinger, U. Friman-Gayer, B. T. Folsom, A. Gaye, G. Gorini, C. Happe, M. Holl, Y. Kamyshkov, T. Kittelmann, E. B. Klinkby, R. Kolevatov, S. I. Laporte, B. Lauritzen, J. I. Marquez Damian, B. Meirose, F. Mezei, D. Milstead, G. Muhrer, V. Neshvizhevsky, B. Rataj, N. Rizzi, L. Rosta, S. Samothrakitis, H. Schober, J. R. Selknaes, S. Silverstein, M. Strobl, M. Strothmann, A. Takibayev, R. Wagner, P. Willendrup, S. Xu, S. C. Yiu, L. Zanini & O. Zimmer

To cite this article: V. Santoro, K. H. Andersen, P. Bentley, M. Bernasconi, M. Bertelsen, Y. Beßler, A. Bianchi, T. Brys, D. Campi, A. Chambon, V. Czamler, D. D. Di Julio, E. Dian, K. Dunne, M. J. Ferreira, P. Fierlinger, U. Friman-Gayer, B. T. Folsom, A. Gaye, G. Gorini, C. Happe, M. Holl, Y. Kamyshkov, T. Kittelmann, E. B. Klinkby, R. Kolevatov, S. I. Laporte, B. Lauritzen, J. I. Marquez Damian, B. Meirose, F. Mezei, D. Milstead, G. Muhrer, V. Neshvizhevsky, B. Rataj, N. Rizzi, L. Rosta, S. Samothrakitis, H. Schober, J. R. Selknaes, S. Silverstein, M. Strobl, M. Strothmann, A. Takibayev, R. Wagner, P. Willendrup, S. Xu, S. C. Yiu, L. Zanini & O. Zimmer (2024) The HighNESS Project at the European Spallation Source: Current Status and Future Perspectives, Nuclear Science and Engineering, 198:1, 31-63, DOI: 10.1080/00295639.2023.2204184

To link to this article: https://doi.org/10.1080/00295639.2023.2204184

Published online: 12 Jul 2023.

NUCLEAR SCIENCE AND ENGINEERING · VOLUME 198 · 31–63 · JANUARY 2024

DOI: https://doi.org/10.1080/00295639.2023.2204184

The HighNESS Project at the European Spallation Source: Current Status and Future Perspectives

V. Santoro,[a]* K. H. Andersen,[b] P. Bentley,[a] M. Bernasconi,[c] M. Bertelsen,[a] Y. Beßler,[d] A. Bianchi,[a] T. Brys,[a] D. Campi,[c] A. Chambon,[e] V. Czamler,[f] D. D. Di Julio,[a] E. Dian,[g,h] K. Dunne,[i] M. J. Ferreira,[a] P. Fierlinger,[j] U. Friman-Gayer,[a] B. T. Folsom,[a,c] A. Gaye,[a] G. Gorini,[c] C. Happe,[d] M. Holl,[a] Y. Kamyshkov,[k] T. Kittelmann,[a] E. B. Klinkby,[e] R. Kolevatov,[l] S. I. Laporte,[c] B. Lauritzen,[e] J. I. Marquez Damian,[a] B. Meirose,[i,m] F. Mezei,[g] D. Milstead,[i] G. Muhrer,[a] V. Neshvizhevsky,[f] B. Rataj,[a,m] N. Rizzi,[e] L. Rosta,[h] S. Samothrakitis,[n] H. Schober,[a] J. R. Selknaes,[a] S. Silverstein,[i] M. Strobl,[m] M. Strothmann,[d] A. Takibayev,[a] R. Wagner,[f] P. Willendrup,[a,e] S. Xu,[a] S. C. Yiu,[h] L. Zanini,[a] and O. Zimmer[f]

[a]*European Spallation Source ERIC, Lund, Sweden*
[b]*Oak Ridge National Laboratory, Oak Ridge, Tennessee*
[c]*University of Milano-Bicocca, Milano, Italy*
[d]*Forschungszentrum Jülich, Germany*
[e]*DTU Physics, Technical University of Denmark*
[f]*Institut Laue-Langevin, Grenoble, France*
[g]*Mirrotron Ltd, Budapest, Hungary*
[h]*Centre for Energy Research, Budapest, Hungary*
[i]*Stockholm University, Stockholm, Sweden*
[j]*Technical University Munich, Garching, Germany*
[k]*The University of Tennessee, Department of Physics and Astronomy, Knoxville, Tennessee*
[l]*ESS consultant, Norway*
[m]*Lund University, Lund, Sweden*
[n]*Paul Scherrer Institut, PSI Villigen, Switzerland*

Received November 22, 2022
Accepted for Publication April 14, 2023

Abstract — *The European Spallation Source (ESS), presently under construction in Lund, Sweden, is a multidisciplinary international laboratory that, once completed at full specifications, will operate the world's most powerful pulsed neutron source. Supported by a 3 M Euro Research and Innovation Action within the European Union Horizon 2020 program, a design study (HighNESS) is now underway to develop a second neutron source located below the spallation target. Compared to the first source, which is located above the spallation target and designed for high cold and thermal brightness, the new source is being optimized to deliver higher intensity and a shift to longer wavelengths in the spectral regions of cold neutrons (CNs) (2 to 20 Å), very cold neutrons (VCNs) (10 to 120 Å), and ultracold neutrons (UCNs) (> 500 Å). The second source consists of a large liquid deuterium moderator to deliver CNs and serve secondary VCN and UCN sources, for which different options are under study. These new sources will boost several areas of condensed matter research and will provide unique opportunities in fundamental physics. The HighNESS project is now entering its last year, and we are working toward the Conceptual Design Report of the ESS upgrade. In this paper, results obtained in the first 2 years, ongoing developments, and future perspectives are described.*

Keywords — *Neutron sources, ultracold neutrons, very cold neutrons, neutron instrument, NNBAR.*

Note — *Some figures may be in color only in the electronic version.*

*Email: Valentina.Santoro@ess.eu

I. INTRODUCTION

The European Spallation Source (ESS) is presently under construction in Lund. At full specification, it will be the most powerful spallation neutron source in existence. Neutrons are produced by the interaction of a 2-GeV proton beam with a tungsten spallation target. To serve the neutron instruments, the energy of the neutrons exiting the target is reduced from mega-electron-volt to milli-electron-volt range, using appropriate neutron moderators. In its initial suite, ESS will have 15 instruments for neutron scattering, with the accelerator planned to reach 2 MW of time-averaged power in the initial years of operation, with a future upgrade to 5 MW. All the planned instruments—in different fields of neutron scattering such as diffraction, small-angle neutron scattering (SANS), imaging, reflectometry, and spectroscopy—are designed to attain world-leading performance at final specifications.

The first 15 instruments will use neutrons from a moderator system placed above the spallation target, using water and liquid parahydrogen for thermal neutrons and cold neutrons (CNs), respectively.[1] However, the ESS facility was designed with the potential to add more instruments thanks to a grid of 42 beam ports for neutron extraction, spanning an angular range of 240 deg, and to the presence of upgrade areas (i.e., locations kept available for the placement of additional instruments). Other key aspects for the future upgrade of ESS are provision for the insertion of a second moderator system below the spallation target and a beam extraction system that has been designed with the capability of extracting low-energy neutrons from either above or below the target. This configuration gives tremendous potential for upgrades at ESS because it offers the possibility to install a second source system, with different features from the first one, as well as the possibility to conceive and design a new set of different instruments, broadening the capability that ESS can offer to the scientific community.

The goal of HighNESS,[2,3] a European Union–funded 3-year project started in October 2020, is to perform a design study of this second source, including a set of neutron scattering instruments and the fundamental physics experiment NNBAR[4,5] (a search for neutron-antineutron oscillations) that will make use of the new source. For the initial instrument suite, the focus was on a source capable of delivering a high brightness of thermal neutrons and CNs. Conversely, the new sources being designed in the HighNESS project will focus on two different aspects: an increase in the total number of neutrons emitted from the source (source intensity) and a shift of the wavelength range toward colder neutrons. A more intense source requires larger moderators and emission surfaces to increase the count rate for instruments or experiments that need high flux. To have a source of colder neutrons, in the HighNESS project, we foresee the need for a very cold neutron (VCN) source and an ultracold neutron (UCN) source (in addition to the second CN source). This upgrade will allow ESS to offer to the scientific community an extremely broad range of neutron energies, from thermal to UCN, enabling a broad range of applications and experiments.

The HighNESS project is structured in ten different work packages (WPs) as shown in Fig. 1. Work Package 1 (WP1) is "Project Coordination" of all activities within the project. Work Package 2 (WP2), "Software Development," has the scope to develop the computational tools needed to study and design high-intensity moderators. These tools will rely on the experimental measurements performed in Work Package (WP3), "Material Characterization with Neutrons," that provide the material property data needed to generate thermal neutron scattering kernels and to validate models. Work Package 4 (WP4), "Moderator Design," and Work Package (WP6), "Advanced Reflectors," represent the core of the neutronic design of the CN, VCN, and UCN sources. These two WPs will need input and requirements from the two scientific WPs—Work Package 7 (WP7), "Condensed Matter Science," and Work Package 8 (WP8), "Fundamental Physics," to ensure that the sources to be designed deliver neutron fluxes and spectra appropriate for performing new and groundbreaking scientific measurements at ESS that cannot be performed with the high-brightness parahydrogen moderator.

During this conceptual design study, there is a continuous exchange of information between WP4 and WP6, and Work Package 5 (WP5), "Engineering," expected to deliver a manufactural mechanical design. All software and data developments performed by WP2 and WP6 will be made available to the public by a cloud-computing resource developed by Work Package 9 (WP9), "Computing Infrastructure." Finally, Work Package 10 (WP10), "Dissemination and and Outreach," will handle the dissemination of all the scientific content produced within this project. In the next sections, highlights are given from each WP (except WP1 and WP10,

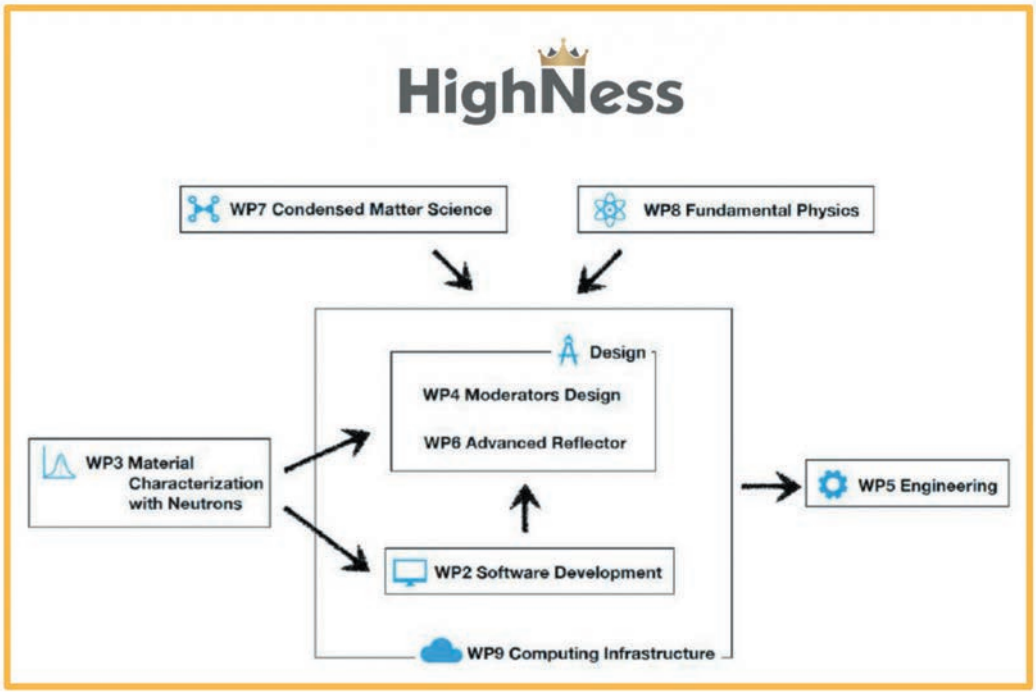

Fig. 1. HighNESS project WP structure.

which will be discussed in later publications) covering the developments made during the first 2 years of the project.

II. SOFTWARE DEVELOPMENT

The accuracy of Monte Carlo simulations, used for the design of moderator reflector systems, depends critically on the thermal neutron scattering libraries used as input to the simulations. Most of the thermal scattering libraries (TSL) in modern evaluations are created using the NJOY[6] code framework. A major limitation of this approach is that such libraries are limited both in the physics and the materials that are currently supported by NJOY, which is primarily aimed at reactor applications. Within the HighNESS project, several of the materials of interest facilitate neutron transport through specific processes, such as SANS and magnetic scattering, and require new developments to make it possible to perform design studies. Thus, the main aim of WP2 is the development of new software tools for the simulation of low-energy neutrons in the novel materials of interest for HighNESS. This includes magnesium hydride (MgH_2), nanodiamond (ND) particles [in collaboration with WP6 (see Sec. VI)], clathrate hydrates, and intercalated graphite. The software is to be used by WP4 and WP6 for simulations of the advanced moderator reflector concepts. Experimental data collected in collaboration with WP3 are also used for benchmarking of the software. In addition, the main inputs to these software tools are being developed through detailed molecular modeling techniques.

The first year of the project focused on the development of the software tools for MgH_2 and ND particles. In the case of MgH_2, and the closely related material magnesium deuteride, we developed NJOY+NCrystal,[7] which greatly extends the functionality of NJOY for polycrystalline materials using a direct interface to NCrystal.[8] In addition, the tool allows for the construction of libraries in a mixed elastic format, thus bypassing one of the major limitations with libraries created with the standard NJOY package, which previously supported either coherent elastic or incoherent elastic cross sections, but not both, in the same file.

For the ND particles, we investigated an alternative approach where instead of using TSL, NCrystal was called on the fly during a Monte Carlo simulation. For this purpose we interfaced NCrystal with the code OpenMC.[9] The SANS physics was included through the creation of an NCrystal plug-in,[10,11] in collaboration with WP6. We also investigated the impact of the finite size of the ND particles on the neutron scattering cross section through detailed molecular dynamics calculations.[12]

Work is now underway on the intercalated graphites and clathrate hydrates. In the following, we give a status update of the current work on clathrate hydrates, in particular, tetrahydrofuran (THF) and deuterated tetrahydrofuran (TDF) hydrates, and oxygen-containing clathrate hydrates.

II.A. Calculation of the Phonon Density of States for Clathrate Hydrates

To build the Type II THF clathrate hydrate structure, coordinates were taken from Ref. [13] in which ab initio optimized structures of THF and H_2 binary clathrates are provided, using the clathrate hydrate structure from Ref. [14]. H_2 was removed from the primitive cell, and a conventional unit cell was built, resulting in 136 water molecules and 8 THF molecules. The structure was then optimized ab initio, using the Perdew-Burke-Ernzerhof functional[15] and Goedecker-Teter-Hutter pseudopotentials[16] with the Grimme D3 correction for van der Waals interactions[17] within the CP2K software.[18] The triple zeta valence plus polarization Gaussian basis set was used, with a cutoff of 1000 Ry. Tight convergence criteria were imposed on account of required accuracy in determining the forces. The resulting optimized structure is shown in Fig. 2. Small displacements from the equilibrium geometry were then generated, and force constants were computed using Phonopy[19] and CP2K. From these, the projected density of states (DOS) was obtained for each element (Fig. 2). To obtain the phonon DOS for the deuterated systems (TDF/H_2O, THF/D_2O, and TDF/D_2, not shown), the corresponding atomic masses were modified, and the phonon calculations were rerun using the same ab initio optimized structure and forces.

II.B. Neutron Scattering Cross Sections of Clathrate Hydrates

The crystalline structure and the DOS of THF/TDF-clathrate hydrates obtained from ab initio density functional calculations were fed into the data processing tool NCrystal,[8,20,21] to generate the neutron scattering cross sections $\sigma_s(\lambda)$ and the scattering kernels $S(Q,\omega)$, where λ is the neutron wavelength and with Q and $\hbar\omega$ representing the neutron wave vector and energy transfers, respectively. The calculated $\sigma_s(\lambda)$ and $S(Q,\omega)$ of THF/TDF-clathrate hydrates at 5.0 K are illustrated in Figs. 3 and 4. Since the incoherent scattering cross section of deuterium is much smaller than that of hydrogen, the Bragg edges resulting from the coherent elastic effects dominate in the case of TDF-clathrate hydrates. The generated $\sigma_s(\lambda)$ and $S(Q,\omega)$ are used further in the Monte Carlo neutron transport codes OpenMC[9] and McStas[22,23] to simulate the transmission measurements of clathrate hydrates performed at Institut Laue-Langevin (ILL) in Grenoble and Paul Scherrer Institut (PSI) in Villigen, Switzerland. The validation of the generated $\sigma_s(\lambda)$ and $S(Q,\omega)$ is ongoing.

The oxygen-containing clathrate hydrates are reported to be a promising VCN moderator thanks to their paramagnetic effects.[24] The theoretical paramagnetic scattering physics is implemented using a plug-in for NCrystal named MagScat,[25] which allows for the calculation of magnetic-scattering cross sections $\sigma_{mag}(\lambda)$, as shown in Fig. 5. The magnetic downscattering cross section $\sigma_{mag,-}(\lambda)$ has a cutoff at $\lambda = 14.3$Å ($E = 0.4$meV), as downscattering can happen only if the incident neutron energy is greater than the zero-field splitting constant.

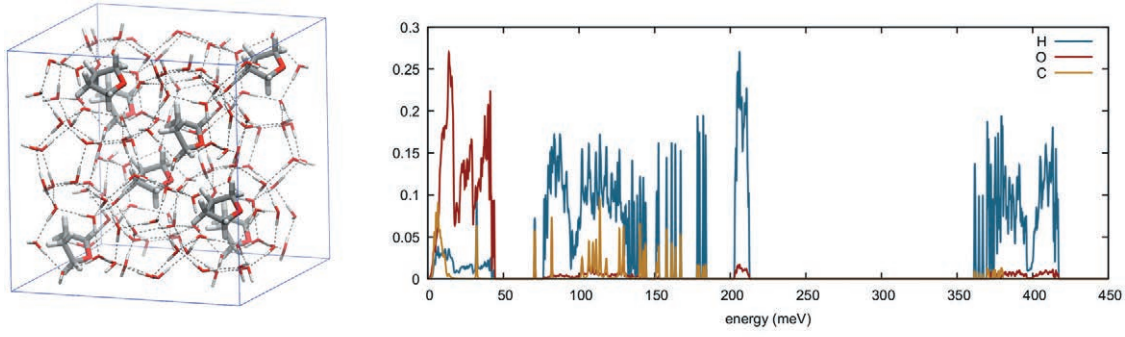

Fig. 2. (a) Structure of the Type II THF clathrate hydrate as optimized by Density Functional Theory. (b) Corresponding phonon DOS for each atom type, normalized to the number of atoms in the unit cell.

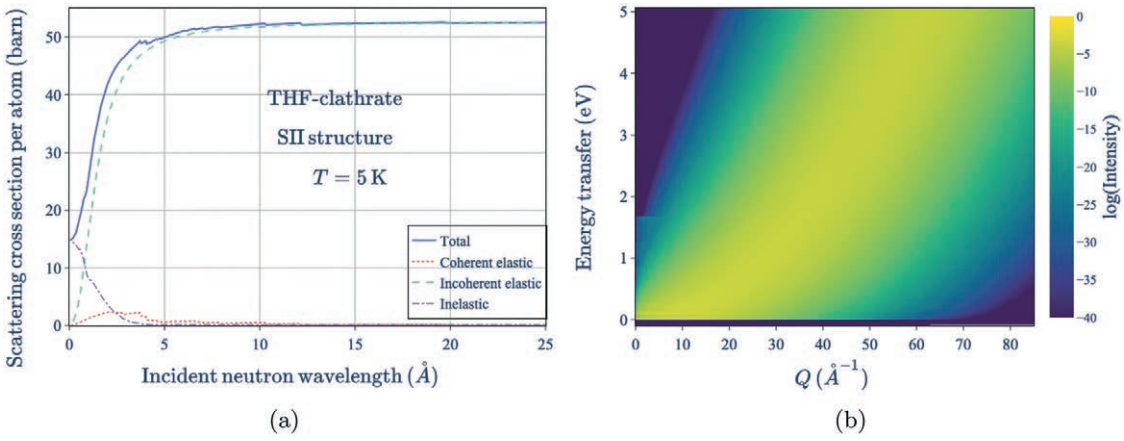

Fig. 3. (a) Different components of the neutron scattering cross sections per atom of THF clathrate hydrates at 5.0 K. (b) The corresponding scattering kernel $S(Q, \omega)$.

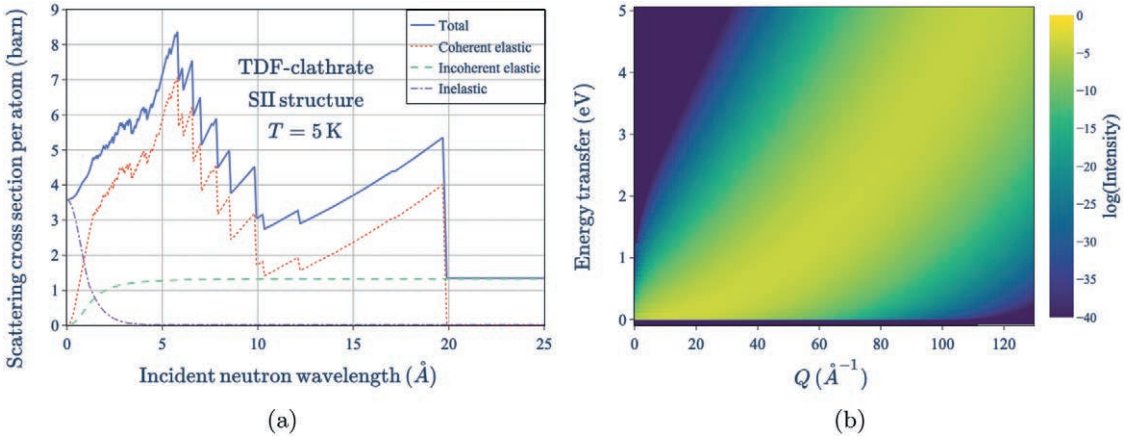

Fig. 4. (a) Different components of the neutron scattering cross sections per atom of TDF clathrate hydrates at 5.0 K. (b) The corresponding scattering kernels $S(Q, \omega)$.

III. MATERIAL CHARACTERIZATION WITH NEUTRONS

The objective of WP3 is to characterize neutron scattering properties of materials that promise large gains in the moderation of CNs down to the energy range of VCNs. Moderators based on such materials are expected to enhance the capabilities of numerous neutron scattering techniques, as well as the reach of particle physics experiments employing beams of slow neutrons. The positive effects of longer neutron wavelengths λ on the performance of various neutron scattering instruments result from the λ dependencies of the instrumental resolution at fixed geometry and the intensity at a fixed resolution [e.g., λ^{-1} and λ^{-2} for reflectometers, λ^{-3} and λ^{2} for time-of-flight (ToF) instruments, or λ^{-3} and λ^{3} for neutron spin echo].[26] Particle physics experiments capable of utilizing higher VCN fluxes include the neutron-antineutron oscillation experiment NNBAR (see Ref. [27]) for which the respective figure of merit (FOM) is proportional to λ^{2}, as well as a projected in-beam search for a nonvanishing neutron electric dipole moment.[28] Experiments searching for new fundamental forces[29] would also profit.

In the initial HighNESS proposal (see Ref. [2]), two approaches were suggested to achieve these intense VCN fluxes. The first approach (discussed in Sec. IV.B) devises an extraction of VCN from the cold source by using advanced reflector materials. The second one foresees a dedicated VCN source consisting of a novel material with a higher VCN production performance than liquid deuterium (LD_2), for which deuterated clathrate hydrates[30] have been identified as particularly promising.

Thanks to their very large unit cells, this material class promises extraordinarily large albedos for the entire CN range. The moderation capability of deuterated

clathrate hydrates is due to low-energy modes of guest molecules, which occupy cages formed in a crystalline network of hydrogen-bonded water molecules in these so-called inclusion compounds. Of particular interest is a binary clathrate hosting oxygen and THF as guest molecules, wherein the molecular oxygen provides an additional path for neutron slowdown.[24] As visible in Fig. 5, this results in a suitable cross section for inelastic incoherent neutron scattering by local modes, which can remove energy from CN without the kinematic restrictions imposed by a dispersion relation.

Work Package 3 is dedicated to characterizing various clathrate hydrates with neutrons to investigate their suitability for potential use in a future upgrade of the ESS. At its core is an extensive experimental program conducted on various instruments of the ILL in Grenoble and PSI in Switzerland. These experiments allow studying the structure and dynamics and measuring the total cross section of this class of materials.

III.A. Manufacturing Procedures and Neutron Diffraction

A central aspect of the entire experimental campaign, as well as for any future application of clathrate hydrates for novel VCN moderators, is a reliable and reproducible manufacturing method for large quantities of material. The production of gas hydrates has been discussed intensively for more than a decade in the context of storing and transporting hydrogen and natural gas (see, e.g., Refs. [31] and [32]). A first series of experiments was conducted on samples of THF-water-hydrates ($17H_2O \cdot C_4H_8O$), which can be prepared relatively easily by stoichiometric mixing of the two liquid starting materials (THF and water) and subsequent cooling below solidification. Neutron diffraction experiments on the ILL's high-intensity two-axis diffractometer D20 showed that clathrates form with almost no residual ice phases. However, the production of binary clathrates hosting both O_2 and THF as guest molecules is more challenging, due to the high pressure required for the O_2 to diffuse into the cage structure. Within WP3, we are working on different strategies to manufacture THF-O_2-hydrates with an evenly distributed grain size and reliable cage filling with O_2. Both quantities will be determined by neutron diffraction techniques.

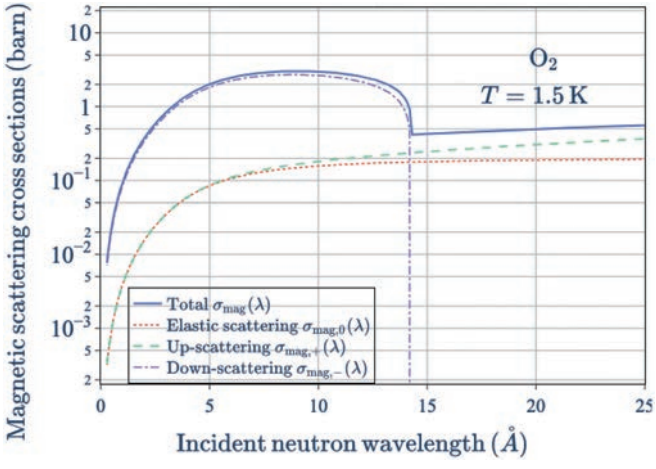

Fig. 5. Magnetic scattering cross sections of oxygen-containing clathrate hydrates at 1.5 K.

III.B. ToF Spectroscopy

Earlier experiments[33] had shown that methane and THF clathrates possess a rich spectrum of incoherent low-energy excitations, but they provided the neutron scattering function $S(q,\omega)$ only in arbitrary units. The results in the aforementioned experiment gave the neutron scattering function $S(q,\omega)$ only in arbitrary units. The measurements within WP3 are devised to determine $S(q,\omega)$ of THF clathrate hydrates in absolute units for all four combinations of full or no deuteration of the water network and the guest molecules, respectively (see Fig. 6). The plot shows the spectra of different combinations of protonated and deuterated components, which allows for a contrast variation to distinguish contributions from the guest molecules and the host lattice. Experiments were conducted in 2021 using the ILL ToF instruments IN5 and Panther, with incident neutron wavelengths of 2 and 3 Å on IN5; and 1 and 2 Å on Panther. While this experimental campaign was focused on clathrates hosting only THF as a guest molecule, future experiments will investigate the dynamics of binary THF-O_2 clathrate hydrates, focusing on the excitations of the confined molecules.

III.C. Determination of the Total Cross Section by Neutron Transmission

The aforementioned experiments are complemented by neutron transmission experiments in the very-cold wavelength range. They serve for characterization of neutron transport through the potential moderator materials and determine the depth from which VCN can be extracted to a beam. From the neutron transmission, one can derive the total cross section of the material.

Denoting by Z^0 the count rate at a detector with no sample, the count rate after insertion of a sample of thickness d is

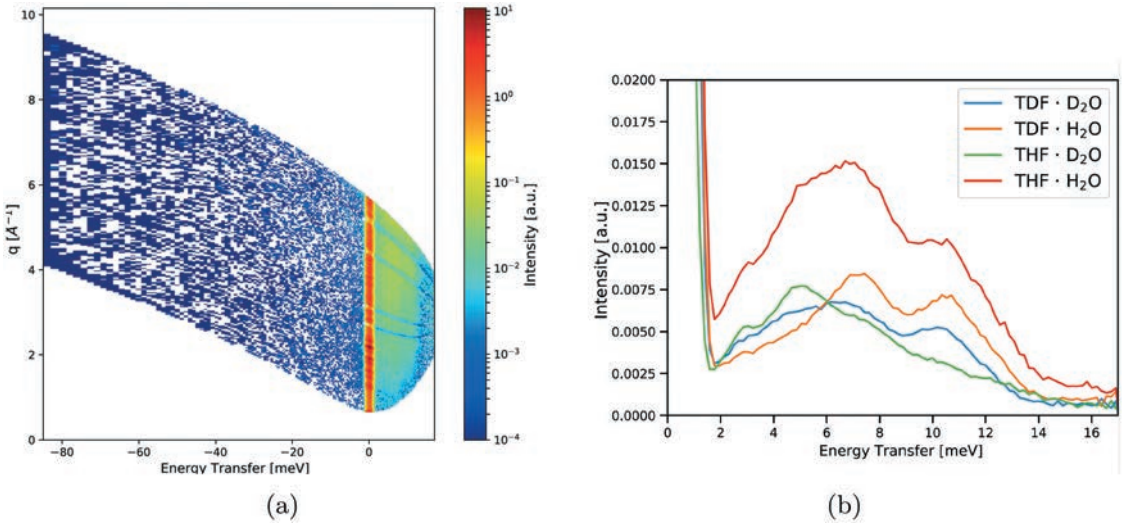

Fig. 6. (a) The neutron scattering function $S(q,\omega)$ measured at ILL's Panther, with an incident energy E_i=19 meV and a temperature of T = 1.4 K. (b) Averaging over q gives an excitation spectrum.

$$Z^+ = Z^0 \cdot \exp(-N\sigma_t d) \ . \tag{1}$$

This is illustrated in Fig. 7. The transmission of the sample can be defined as $T = \frac{Z^+}{Z^0}$, which allows the total cross section σ_t to be expressed as

$$\sigma_t = \frac{1}{Nd}\ln\left(\frac{1}{T}\right) = \frac{1}{Nd}\ln\left(\frac{Z^+}{Z^0}\right) \ . \tag{2}$$

A ToF setup allows us to measure these quantities as a function of the neutron's wavelength λ. Experiments in the CN and VCN range were and are to be conducted at the ILL and the PSI. This allows for the determination of the transparency of the material for VCN as well as a wide range of Bragg edges in the CN range.

IV. MODERATOR DESIGN

Central to the HighNESS project is the WP dedicated to the moderator design, WP4. The goal of this WP is to produce the neutronic design of CN, VCN, and UCN sources. The energy and wavelength ranges for the three sources are shown in Table I.

IV.A. Cold Neutron Source

In the first part of the HighNESS project, the effort was concentrated on defining FOMs for the design of the moderators, and on the design of the CN source, a high-intensity LD_2 moderator.

For the first task, the definition of the FOM considers that the sources are intended for several classes of applications, namely, for neutron scattering instruments for condensed matter research and fundamental physics experiments studied in WP7 and WP8, respectively. The conventional range for neutron scattering experiments is between 2 and 20 Å. However, this range has been extended up to 40 Å, to cover a region in the VCN, as yet relatively unexplored but of potential interest for neutron scattering. This is particularly interesting for SANS and spin-echo instruments, for which novel concepts using longer-wavelength neutrons are being studied within the project. It was therefore decided that the design of the moderator should be optimized by monitoring the intensity from the emission surface integrated

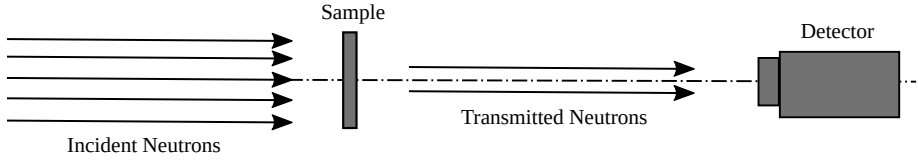

Fig. 7. Illustration of the transmission measurements conducted in the CN and VCN range. Adapted from Ref. [34].

TABLE I

Neutron Classification

Type	Wavelengths (Å)
Cold neutrons	2 to 20
Very cold neutrons	10 to 120
Ultracold neutrons	> 500

over wavelengths between 2.5 and 40 Å to include both CN and (partially) VCN. Concerning the FOM for fundamental physics, the main focus is on the NNBAR experiment, for which the sensitivity of the experiment is proportional to the number of neutrons multiplied by the square of the ToF. Hence, the FOM is given by the intensity from the emission surface weighted by the wavelength squared and integrated between 2.5 and 15 Å.

With these considerations in mind, the design of the high-intensity LD_2 moderator must simultaneously accommodate several instruments. An intensive optimization process was carried out to study a configuration where the NNBAR and neutron scattering instruments are placed on two opposite sides of the facility. The resulting design, for which an engineering study is currently being carried out by WP5, is shown in Fig. 8. The moderator is box-shaped, with a large opening—24 cm high, 40 cm wide—on the side facing the large NNBAR slot for maximum emission of neutrons (NNBAR side), and a smaller opening—15 cm high, 15 cm wide—on the opposite side for neutron scattering experiments (WP7 side). It was found that the presence of a cold (< 77 K) beryllium filter-reflector placed on the NNBAR side increases the NNBAR FOM by about 30%. The WP7 side contains a reentrant hole for neutron extraction from the depth of LD_2 at which the flux is at maximum. The reentrant hole gives an increase of the WP7 FOM of about 35%.

The intensity and the brightness of the LD_2 moderator as a function of wavelength is compared with the upper flat parahydrogen moderator in Fig. 9. For the calculation for the lower moderator, we assumed the presence of aluminum inside the vessel corresponding to an amount of 2.5 vol % and a LD_2 temperature of 22 K. Note the effect of the Be filter/reflector on the spectra for the NNBAR opening. The high performance comes at the cost of high heat load on the cryogenic parts of the moderator (about 50 to 60 kW), for which the feasibility of the cooling is being studied by WP5 (see Sec. V).

IV.B. VCN Source

The second type of source under study in HighNESS is intended to produce VCN. In the original proposal, two approaches were considered for the design of such a source. One involves a dedicated VCN source made of a material with a higher VCN production performance than LD_2[2] while another one involves the extraction of

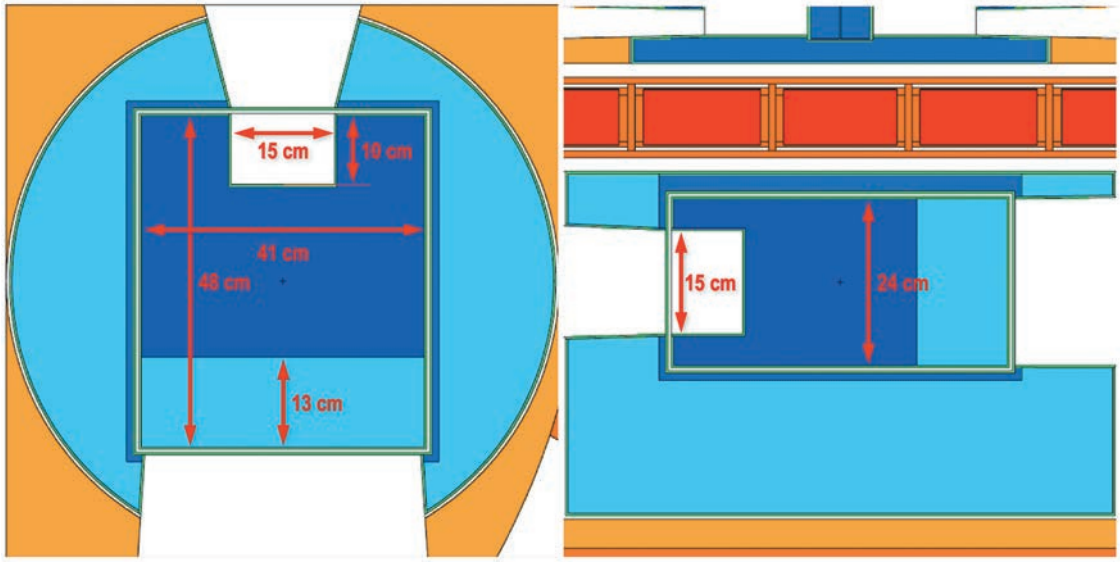

Fig. 8. Liquid deuterium moderator. (a) View from above. (b) View in the proton beam direction. Color scheme—dark blue: liquid deuterium; blue: water premoderator; light blue: beryllium; green: aluminum cladding; orange/dark orange: steels; red: tungsten target.

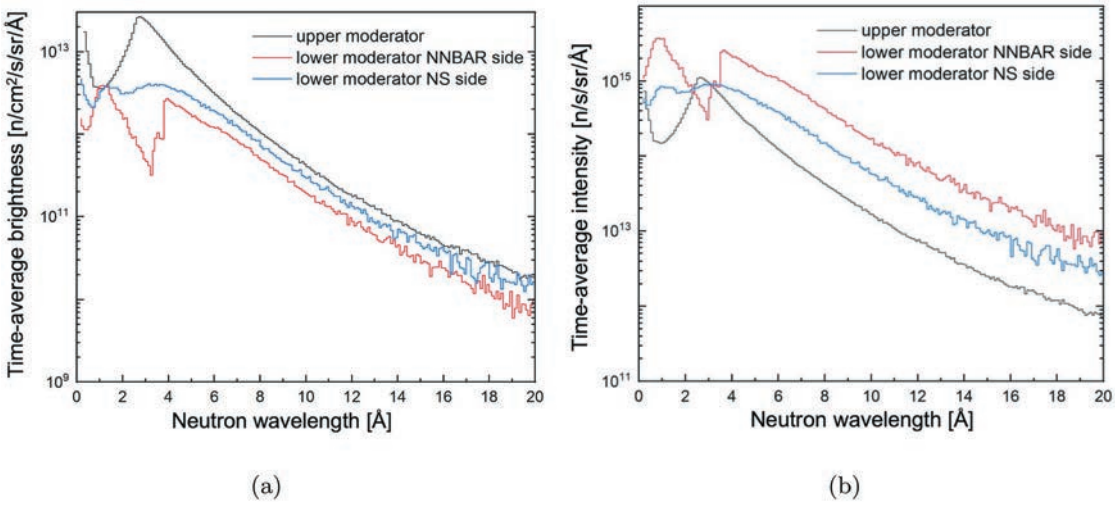

Fig. 9. Comparison of (a) spectral brightness and (b) intensity of upper and lower moderators, at 5-MW average power. The spectra for the upper moderator are the average over the 42 beam ports.[1] For the lower moderator, calculated spectra are shown for two openings (i.e., for the NNBAR and WP7 neutron scattering experiments).

VCN from the cold source by using advanced reflectors. This section focuses on the first of the two options, where solid ortho-deuterium (SD_2) was found to be the best material to replace LD_2 as a dedicated VCN source. For the second option, a dedicated experiment, to be performed at the Budapest Neutron Center[a] (BNC), will assess the effect on VCN flux when utilizing a small extraction channel coated with a layer of NDs. A third design option was suggested by Nesvizhevsky,[27] which consists of a hybrid design using LD_2 and SD_2 as well as ND to improve the reflection of VCN.

Our investigation started from the study of the performance of a moderator placed below the spallation target (thus replacing the baseline LD_2 moderator described in Sec. IV.A), where part of the LD_2 is replaced by SD_2 at 5 K (i.e., considering configurations similar to those suggested in Ref. [27]). It is expected that a SD_2 source will provide notable gains for longer-wavelength neutrons. This effect was studied in a quantitative way for various geometrical configurations. Additionally, we analyzed the effect of adding a layer of ND powder (with an average particle size of 5 nm) surrounding the deuterium as a reflector material. This layer both reduces VCN leakage and increases the effective path length within the source. These calculations could be carried out for the first time thanks to the recent development of TSL for both solid deuterium[35] and NDs[36] in MCNP 6.2.

After testing several possibilities, the best configuration was found to consist of a SD_2 block of the same dimensions as the conventional LD_2 without a reentrant hole on the WP7 side. Both moderator and extraction walls are covered by a 0.5-mm layer of NDs to increase the reflectivity of VCN. Since intensity was lost on the NNBAR side for the range 4 to 10 Å, a 20 K Be filter was inserted outside the moderator's vessel on the same side following the same approach used with the conventional cold source. This filter increases the performance on both the NNBAR and the WP7 sides by 30% and 4%, respectively, while it is detrimental in the VCN range on the NNBAR side, where VCNs are not used as there is a gravitational cut for neutrons with wavelengths exceeding 15 Å. The top view of the geometry is shown in Fig. 10a. As shown in Fig. 10b, order-of-magnitude gains are seen for $\lambda > 40$ Å, along with gains exceeding a factor of 2 from 10 to 40 Å (when comparing against a liquid-deuterium moderator design similar to the conventional CN-source design shown in Fig. 8).

Ongoing discussions with the WP5 team are aiming to solve the problem of cooling a SD_2 block placed so near the spallation target. These discussions led to the conceptualization and preliminary simulations of embedded foamlike aluminum and aluminum-beryllium alloy cooling structures, which improve SD_2 thermal conductivity and, in conjunction with a standard liquid-helium cooling pipe, should allow for a rate of heat extraction capable of keeping the solid deuterium well below its melting point. In particular, the use of beryllium alloys in such cooling structures appears to be more favorable in terms of both cooling (due to reduced self-heating) and neutronics; these should maintain the large gains over a LD_2 moderator reported in the previous paragraph (while pure aluminum foams would likely

[a] https://www.bnc.hu/?q=BRR.

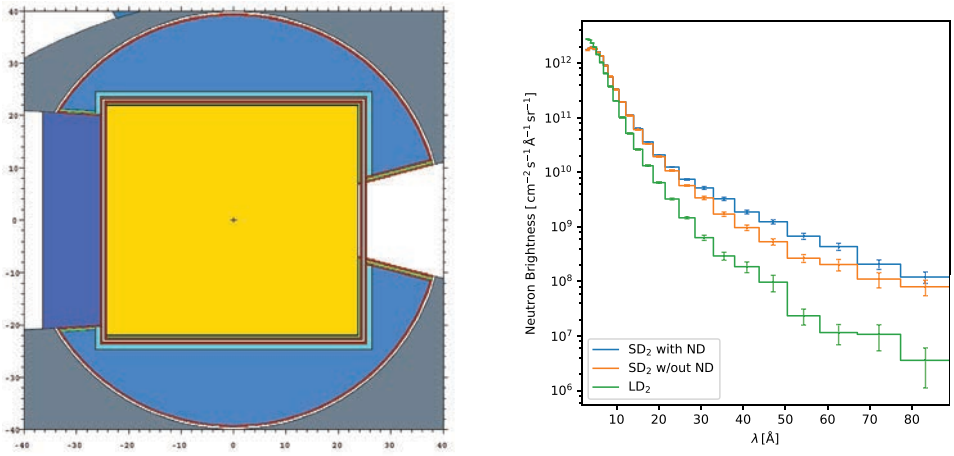

(a) (b)

Fig. 10. (a) Top view of the VCN source (MCNP model). Gray: steel; red: aluminum; cyan: premoderator and reflector light water; light blue: beryllium reflector; blue: cold beryllium filter; gold: SD_2 moderator; green: ND VCN reflector. (b) Brightness spectra comparison for different lower-moderator designs using LD_2, SD_2, and solid deuterium + ND reflection layer.

limit the gains to factors of 4.5 and 1.5 for $\lambda >$ 40 Å and 10 Å to 40 Å neutrons, respectively).

Such an innovative source would be an alternative to the LD_2 source and could be used at a later stage (e.g., after the NNBAR experiment is completed) to provide ESS with a dedicated VCN source while retaining a very large intensity of CNs. This source would offer unprecedented performance in the VCN range, with a brightness of about 1×10^8 n/cm^2·s^{-1}·sr^{-1} at 40 Å, providing opportunities that are currently unavailable in neutron scattering: as predicted, for instance, for reflectometry[37] as well as for spin echo and spectroscopy.[38] Time distributions of CNs (at 5 Å) and VCNs (at 27 Å) are shown in Fig. 11. These indicate that for VCNs, there is a time shift with respect to the duration of the incoming 2.86-ms proton pulse along with widening of the time distributions, but these distributions would still be feasible for ToF measurements. In conclusion, such an option should be considered as a future alternative design of the lower source for ESS and will be further investigated by the WP4 Team.

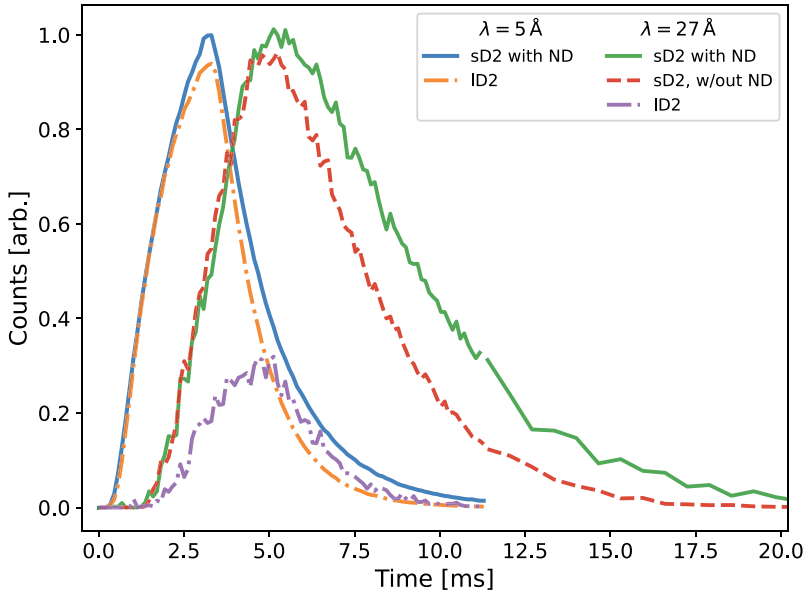

Fig. 11. Temporal response for neutrons at $\lambda = 5$ and $\lambda = 27$Å for the SD_2 moderator with and without ND, as well as the LD_2 moderator. Counts are normalized separately for each wavelength to the maximum value reported among all three moderators.

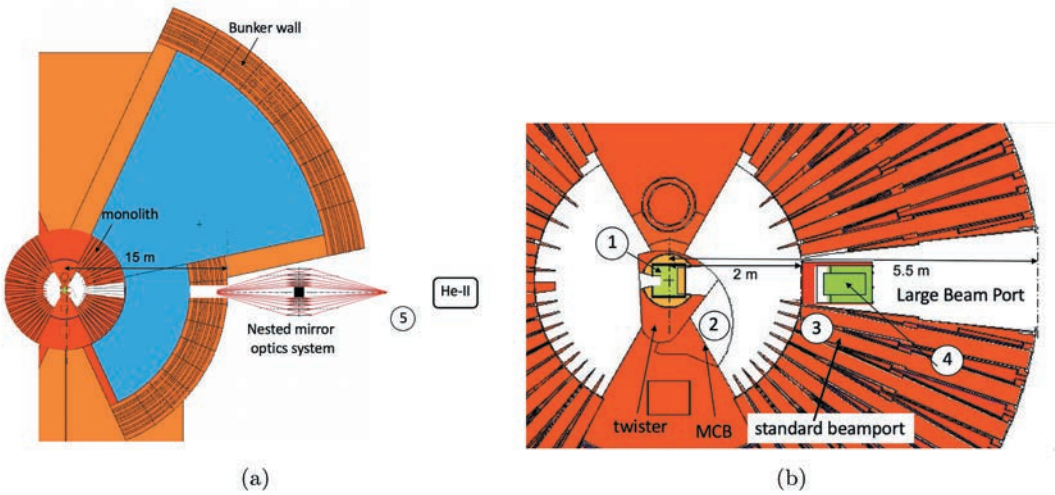

Fig. 12. (a) Horizontal cut through the target region, at the height of the LD_2 moderator (shown in green) situated below the spallation target (not visible). The cylindrical region of 5.5-m radius around the center represents the shielding monolith (shown in red). (b) Magnification of the central part of the figure (a). About half of its 42 standard beam ports are visible in the cut plane.

IV.C. UCN Source

Different possibilities for placement of UCN sources at ESS were identified at the time of writing the HighNESS proposal, and additional ideas were later elaborated at a workshop dedicated to VCN and UCN sources at ESS.[b] An overview of the identified locations is depicted in Fig. 12. The possible locations of UCN sources are (1) inside the "twister"; (2) inside the moderator cooling block (MCB); (3) in a standard beam port; (4) in the NNBAR Large Beam Port (LBP) (shown as a white segment in the monolith); and (5) outside the "bunker," a heavy concrete shielding structure (shown in orange) placed around the monolith—the minimum distance of this location from the moderator is 15 m. The possibilities vary from placing a UCN source directly beneath the spallation target, to in-beam positions placed at 15 m—or farther away—from the target.

Concerning materials for UCN production, it was confirmed at this workshop that the two viable options for converter materials to generate intense UCN densities are superfluid helium (He-II) and SD_2. All the presented options are discussed in detail in Ref. [39].

At the present stage of the project, we have calculated the production rate densities at the proposed different locations (see Fig. 12) to assess the possibilities that ESS can offer for UCN production and compare the options for a high-performing UCN source. Aspects related to the design of the UCN extraction system will also be considered in the last part of the project. The production rate density in He-II and SD_2 as a function of the distance from the cold moderator, from near the moderator surface to 150 cm, is shown in Fig. 13. These estimates are obtained by multiplying the neutron fluxes for the UCN production cross sections,[40–43] without any modeling of the converters; they are therefore representative of the production in He-II or thin SD_2, i.e., of configurations where the perturbation of the incoming cold flux, from the converter itself, is minimal. In the following, we discuss some other promising concepts.

IV.C.1. UCN Source in the LBP

This option (option 4 in Fig. 12) consists of placing a large He-II converter in the ESS LBP, which is a special beam port built for the NNBAR experiment and which spans three standard beam ports; see Ref. [5]. This unique location provides free access for neutron extraction over a large angular range, allowing the installation of a large UCN converter placed close to the center of neutron production.

The LBP is foreseen to first serve the NNBAR experiment and could afterward be exploited for the production of UCNs. A rigorous proposal by Serebrov and Lyamkin[44] foresees a vessel of about 60 L filled with He-II, surrounded by a LD_2 reflector and a lead shield. More details can be found in Refs. [39] and [44]. A preliminary UCN production rate density of about 300 $cm^{-3}{\cdot}s^{-1}$ has been estimated, and the heat load appears to be sufficiently low (about 8 W in He-II) to allow for cooling and maintaining the He-II at the desired temperature.

[b] https://indico.esss.lu.se/event/2810/.

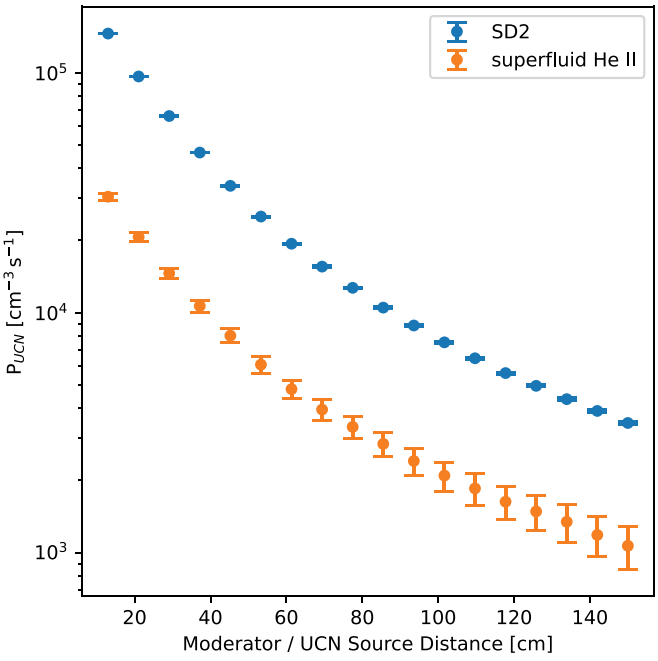

Fig. 13. Calculated production rate densities for He-II[40] and SD_2[43] as a function of the distance from the LD_2 moderator. The listed distances are from the center of the UCN source to the edge of the beryllium filter on the LBP-facing side of the lower moderator.

IV.C.2. UCN Source In-Beam Option Using Nested Mirror Optics

The in-beam option offers the advantage of easier accessibility to the experimental apparatus, more flexibility in the design of the UCN extraction, and lower heat load levels. The best location to place an in-beam UCN source is on the beam axis of the LBP (location 5 in Fig. 12), where the moderator can be viewed under the largest possible solid angle. In this scenario, the source is placed outside the neutron bunker and uses advanced nested mirror optics to extract the neutrons, as described in Ref. [45]. Preliminary calculations for this option give a production rate density of about 200 $cm^{-3}{\cdot}s^{-1}$, which, for a volume of He-II of 120 L, would provide a production rate of 2.5×10^7 s^{-1}. This calculation assumes the use of nested mirror optics[46] with an m value of 6. It should be noted however that these calculations were based on an earlier model of the LD_2 moderator. The latest model, with a more realistic temperature of 22 K and with 2.5% of Al inside the LD_2 moderator vessel, gives an intensity 20% lower than used in Refs. [39] and [45].

IV.C.3. UCN Converter Located in the MCB Position

Another possible location for a UCN converter is inside the MCB shown as position 2 in Fig. 12, which offers the advantage of a high neutron flux, since it is close to the target, and of accessibility using different supply lines. We describe this option in more detail with respect to the previous ones since the conceptual design has not been reported in other publications.

The draft engineering design is being developed within WP5. The concept consists of a three-stage coaxial shell fed from two channels (Fig. 14). The stages are first, the thermal moderation layer (marked red in Fig. 14) with H_2O at room temperature; second, the cold moderator shell consisting of LH_2 or LD_2 at 20 K optimized for a high 8.9-Å yield (marked cyan in Fig. 14); and third, the centered He-II converter (marked blue in Fig. 14). The CNs exiting the LD_2 moderator will be transported by a feeding channel consisting of a neutron guide coated by ND or MgH_2 (marked in yellow in Fig. 14). The UCNs could be extracted from the He-II by either a vertical or a horizontal extraction channel; see Fig. 14.

For the He-II converter in this location, a UCN production rate density of $P_{UCN} \approx 1400$ $cm^{-3}{\cdot}s^{-1}$, considering only the contribution from the LD_2 moderator, can be achieved (see Fig. 13). For this concept, a dedicated MCNP parametric study regarding the dimensioning of the moderators, heat load on the structures, and moderator media is in progress.

IV.C.4. Summary of the Current UCN Work Design

Although the estimates of UCN production rate densities for some of the possible concepts at ESS are still very preliminary, a first comparison to sources that are currently in operation or in design/construction indicates quite promising achievable performances. For example, the in-beam option using nested mirrors would lead to a UCN density of about 6×10^4 cm^{-3}, assuming a He-II temperature of 0.8 K and a corresponding neutron lifetime of 300 s.[45] This performance is comparable to the expected UCN density for the Petersburg Nuclear Physics Institute design for the WWR-M reactor[44] and is not presently achieved by any UCN source in the world. A He-II source placed in the LBP would provide higher UCN densities but would give less freedom in the design of the neutron extraction and more challenges in keeping the temperatures of the He-II below 1 K. Production rate densities closer to the target are even higher, but the expected performance for realistic designs has not been analyzed yet.

IV.D. Outlook

In the remainder of the HighNESS project, activities will continue for all three sources under study. For the

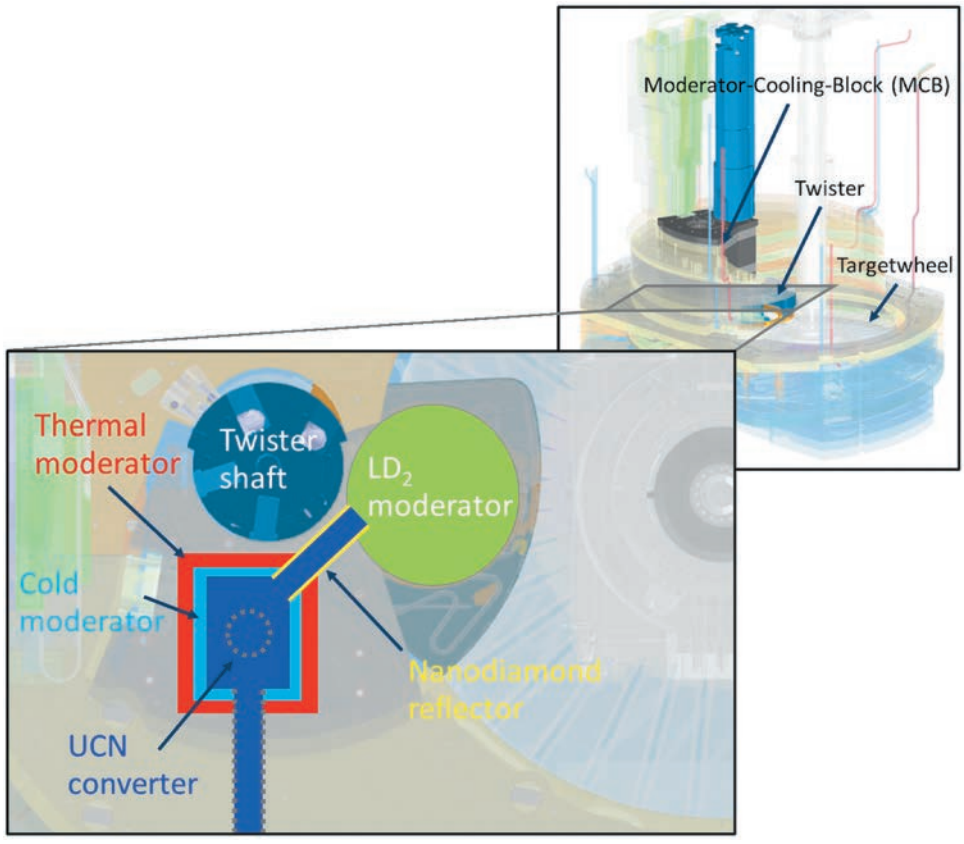

Fig. 14. Conceptual design of a UCN source in MCB position.

CN source, further iterations with the engineering work package WP5 will be carried out to reach the final design. Neutronic analyses are in progress for the VCN and UCN sources, and all the design options, including the new ones identified at the VCN/UCN workshop, are being evaluated. Finally, at the end of the project, the different sources will be integrated into a common design.

V. ENGINEERING

Within the framework of WP5, the engineering implementations of new moderator concepts and beam extraction systems are analyzed. This includes, in particular, computer-aided design (CAD) of the advanced moderator concepts including structural-mechanics and fluid-dynamics simulations, structural materials selection, manufacturability verification, weldability analysis, definition of fluid parameters, cooling process concept design, and verifying the design's integrability into the ESS facility. This section contains the current status of work on WP5.

V.A. Engineering Aspects Related to HighNESS Moderators

The installation of a new neutron source in an existing infrastructure presents several engineering challenges. The selection of the location for future moderators must deal with the fact that the existing structure imposes limitations on the accessibility and exchangeability of components. Figure 15 shows the ESS target monolith. The colored components represent the possible locations for the planned moderator upgrades, for which engineering aspects are under analysis in WP5.

The first moderator support structure, the so-called twister (shown in dark red in Fig. 15), contains a liquid parahydrogen low-dimensional moderator only. This moderator is installed in the upper part of the twister, above the tungsten target wheel. However, the twister design allows for use of the space below the target wheel for future moderator upgrades. This location is characterized by its proximity to the neutron production center and thus by a high neutron yield. The disadvantage is the extraordinarily high heat load caused by the 5-MW proton beam. The baseline design choice in HighNESS is

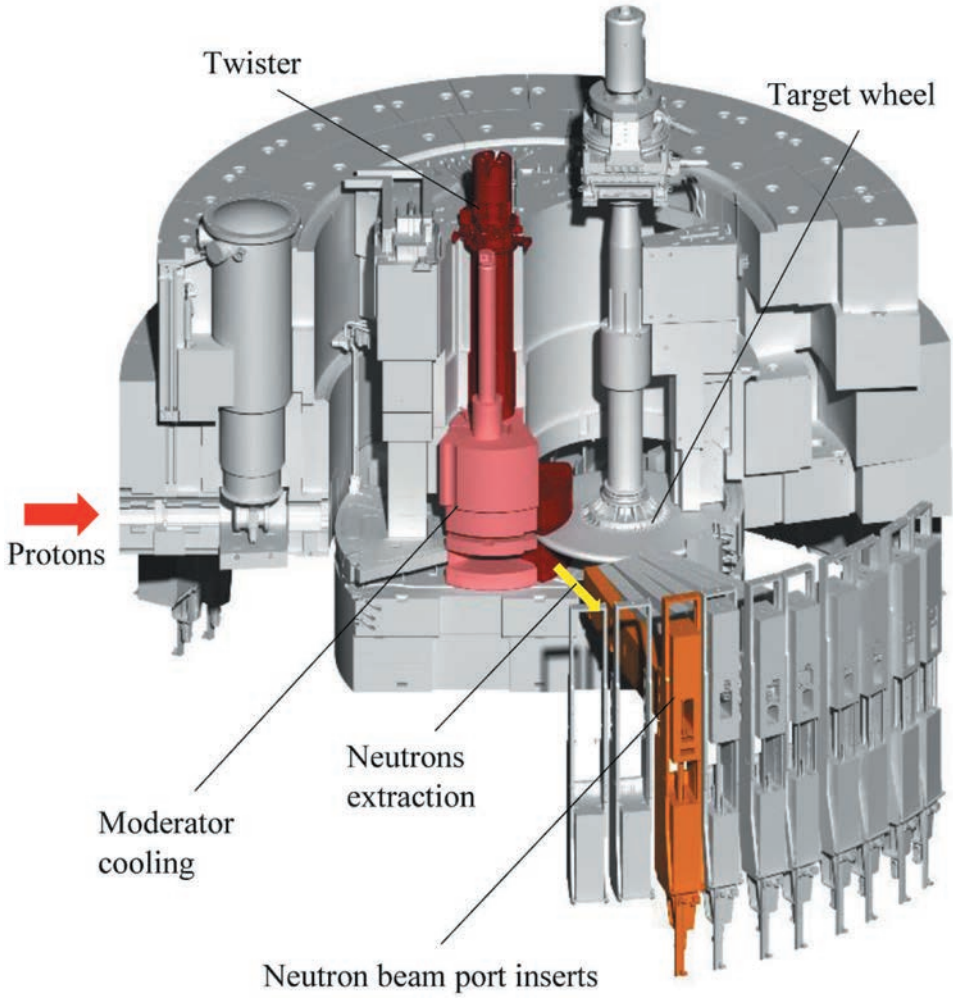

Fig. 15. ESS target monolith with highlighting of some of the possible locations of the HighNESS sources, for which engineering study is ongoing; see also Fig. 12. Dark red: location for the upper parahydrogen and lower LD_2 moderators (twister); light red and orange: possible locations for He-II UCN source, i.e., MCB and neutron beam port inserts, respectively.

to place a voluminous LD_2 moderator, as discussed in Sec. IV. This high-intensity CN source is at the heart of the project, and the engineering design is currently being performed within this WP. As discussed above, a potential future upgrade could be the replacement of the LD_2 moderator with a SD_2 moderator, which would potentially deliver CN, VCN, and UCN from a single source. The high expected heat loads make the cooling of such a source very challenging, and an investigation of its feasibility is planned.

In addition to the twister, the removable shielding blocks near the moderator present possible locations for future moderator upgrades. As previously mentioned, the so-called MCB (light red component in Fig. 15) is particularly attractive for a secondary UCN source placed near the CN source because it is close to the spallation center. Thus, a UCN converter placed inside the MCB would receive a high neutron flux. Additionally, because of its proximity to the high radiation zone, the MCB must be actively cooled; thus, a cooling system is already available and could be adapted for a new source. Finally, this block is exchangeable, and handling devices within the ESS infrastructure are already available. Since the heat load is considerably lower here than within the twister, a UCN source would also be conceivable, and it is currently investigated together with WP4 (see Sec. IV.C.3). Since this option has the highest heat load of the possible locations for UCN and is therefore critical in terms of cooling, it will be further investigated by WP5. However, the choice for the final location of the UCN has not yet been decided.

Another option for the installation of a UCN source is offered by the neutron beam port inserts (shown in

orange in Fig. 15), which can be replaced by a moderator insert or a new type of beam extraction system. The advantage is that the entire cryogenic infrastructure can be installed outside of the monolith. The disadvantage is that such an insert can serve only one instrument at a time. Further locations for a UCN have also been identified, which are explained in more detail in Sec. IV.

V.B. LD_2 Moderator for CNs

The biggest engineering challenge for the CN source is handling the heat load on the LD_2 moderator of about $Q_{heat} = 57$ kW resulting from the spallation process of the 5-MW proton beam. A mass flow of at least $\dot{m} \geq 3400$ g $\cdot s^{-1}$ LD_2 is needed to remove the particle heat and to keep the average temperature increase, as required, below 3 K. The moderator will have a static liquid pressure of $p = 5$ bars, a moderator inlet/outlet temperature of $T_{in/out} = 21/24$ K, and an average moderator temperature of $T_{av} = 22.5$ K. Assuming a flow velocity of up to $w \leq 5\,\mathrm{m} \cdot \mathrm{s}^{-1}$, an inlet/outlet pipe diameter of $d = 70$ mm would be required, which must fit into the existing twister structure. Several iterations with WP4 led to the following preliminary engineering design of the LD_2 moderator. The moderator vessel will be made of high-strength aluminum alloy Al6061-T6, which allows local stresses up to $S_m = 87$ MPa and will be filled with approximately 34 L of LD_2. The cold moderator will be surrounded by a vacuum jacket followed by a light water premoderator and a warm beryllium reflector. In addition, one cold beryllium filter ($T_{\mathrm{BeF}} \leq 80$ K) is installed within the cold moderator vessel on the side facing the large neutron-beam window (blue block in Fig. 16).

The fluid guides ensure that flow separation, dead areas, and swirls do not occur. The extension rods ensure additional mechanical stability since the vessel walls are flat and need to be as thin as possible to minimize neutron losses. The moderator will be milled and partially electrical discharge machined from a solid block of aluminum alloy Al6061-T6, and finally, the cover will be welded to the main body with "low-distortion" electron beam welding.

In addition to the usual structural and fluid mechanics issues, integrability must also be checked since the components must be integrated into an existing source. Originally, the twister was designed for a total moderator volume of about 4 L (2 × 0.65 L for the upper moderators and 2 × 1.3 L for the lower moderators). Integrability is critical because the LD_2 moderator has a substantially larger volume and thus dissipates significantly more heat. Therefore, larger supply and dissipation cross sections are required. All supply lines must be routed through the twister shaft. However, the diameter of the shaft cannot be increased since it is surrounded by nonreplaceable shielding elements. Figure 17 shows the twister with the upper moderator on the leftmost image; on the rightmost image, the integrated volume LD_2 moderator is placed in the lower moderator plug. The final engineering design of the LD_2 moderator is still in progress and will be completed in 2023.

V.C. Engineering Design of the UCN Source

The second engineering subproject in the framework of HighNESS will investigate the integrability of the UCN source into the existing facility. As discussed in Sec. IV.C, currently, neutronic studies are ongoing

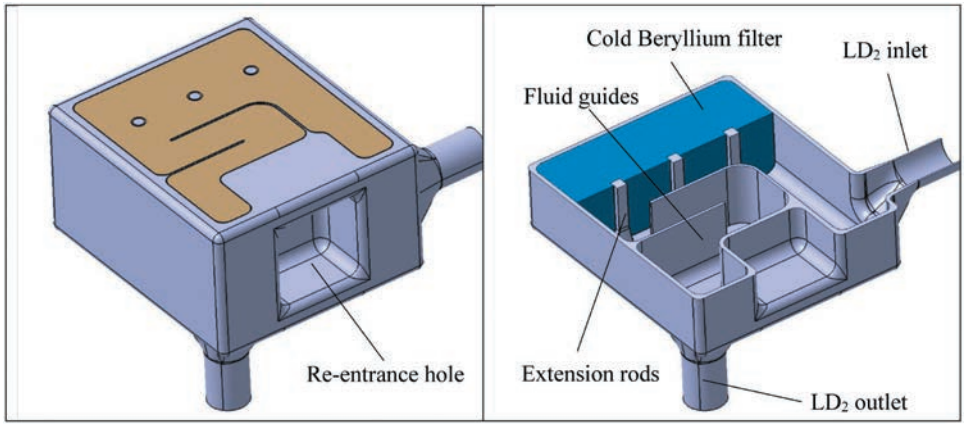

Fig. 16. Preliminary engineering design of LD_2 moderator. See explanation in the text.

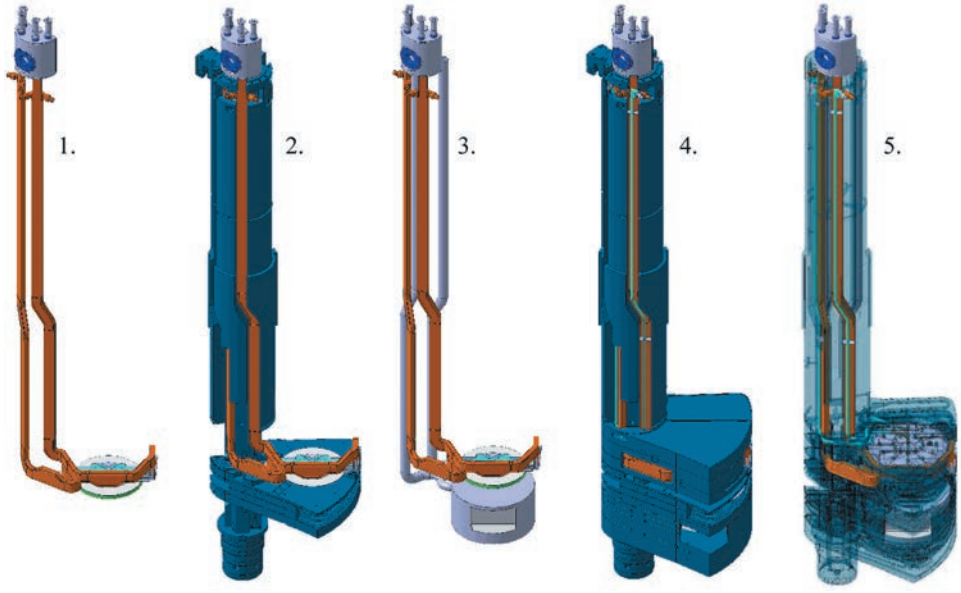

Fig. 17. LD_2 moderator integration. 1. Upper moderator plug; 2. upper moderator plug in the moderator support structure; 3. moderator plug with LD_2 moderator; 4. and 5. moderator plug in the moderator support structure and surrounded by the outer reflector, respectively.

to identify the best location for such a source. The engineering design will be carried out by WP5 on the selected concept.

V.D. Experimental Validations

Two experiments are planned in the near future, related to advanced reflector concepts and UCN materials under study in Highness:

1. Validation of the reflection properties on CN and VCN of ND and MgH_2 layers; measurement performed in collaboration with the BNC.

2. Investigation of the heat transportability and phase stability of ^{4}He in phase-state II (He-II) measured at Forschungszentrum Jülich ZEA-1.

These experiments are done in collaboration among WP4, WP5, and WP6; since the engineering support is given by WP5, they are described in this section.

V.D.1. Prototype Experiment of Moderator Using ND and MgH_2 Advanced Reflectors

This experiment will be performed at the Budapest Research Reactor in the second half of 2023. At the 10-MW research reactor, a moderator test facility is currently under construction in neutron channel 4. The conceptual design of the facility is depicted in Fig. 18. The test station will allow measuring pinhole images of the moderator and ToF neutron spectra.

The moderator setup consists of three interchangeable vessels filled with a 10-mm-thick layer of ND powder, MgH_2 powder and an identical empty vessel for background subtraction, respectively, that will be placed around a hydrogen cold moderator (Fig. 19). The cold moderator is fed by the thermal neutron field diffused by a beryllium cylinder located in the line of sight of beam channel 4 (see also Fig. 22 in Sec. VI). The moderated neutrons of the moderator/reflector assembly are led into a 600-mm-long beam guide surrounded by a 5-mm-thick ND powder layer. The spectra of the reflector/moderator/guide assembly are measured by a pinhole ("camera obscura") ToF two-dimensional detector setup (see Fig. 18). All structures of the setup that are placed in the neutron beam are manufactured of aluminum to minimize neutron absorption and activation. The H_2 supply lines are led into the cryostat system outside the bunker where the LH_2 liquefaction takes place and a defined LH_2 ortho/para ratio can be generated.

V.D.2. Experimental Investigation of He-II Phase Stability Under an Applied Local Heat Load

He-II is one of the two possible materials studied in HighNESS for a UCN source at ESS. For the option of

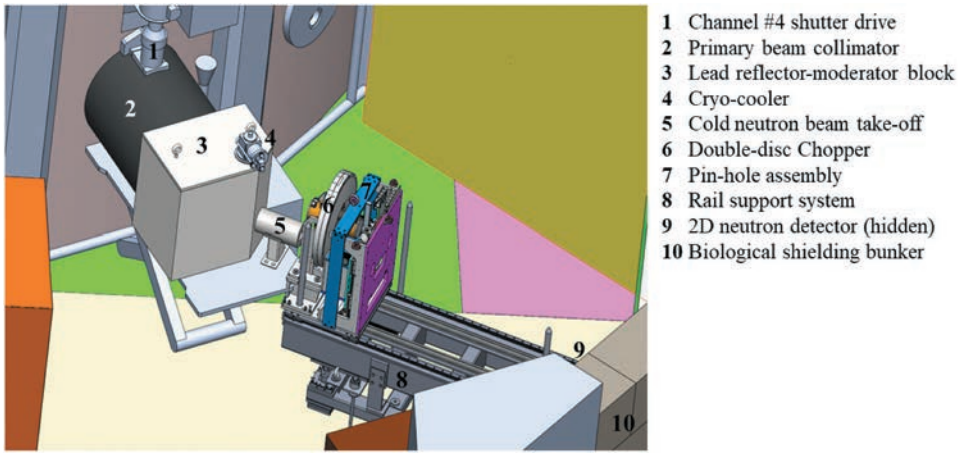

Fig. 18. Sketch of the moderator test facility under construction at the beam channel 4 beamline of the 10-MW Budapest Research Reactor of the BNC.

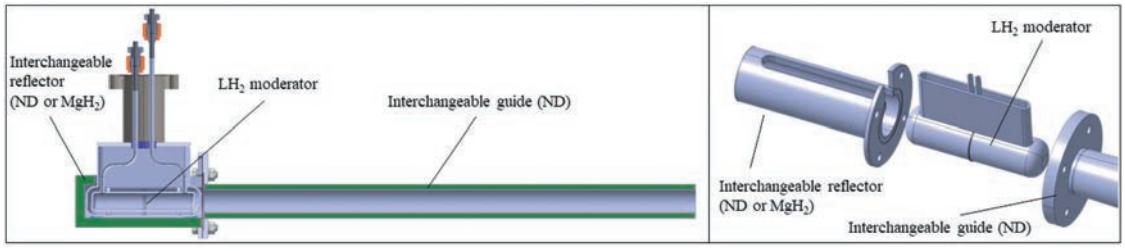

Fig. 19. Experimental moderator/reflector/guide setup with interchangeable configurations placed within the neutron beam.

a He-II converter inside the MCB, because of the close position to the spallation target, a high heat load is expected. Therefore, an experimental investigation of the phase stability of He-II is planned to determine the phase behavior and limit value for a locally induced heat load. The experimental setup consists of a glass vessel placed inside the insulation vacuum of the ZEA-1 laboratory cryostat of Forschungszentrum Jülich. Within the He-II filled vessel, an absorber made of black eloxated aluminum foil is positioned to be decoupled as much as possible from the surroundings (Fig. 20). The absorber is irradiated by a 445-nm laser beam with a maximum power of 500 mW. The oval-shaped beam sized $\sim 0.05 \times 0.2$ mm leads to an maximum heat load of 50 $W \cdot mm^{-2}$, which can be deposited into the He-II. The system is observed through a beam port window to visually detect a phase change.

V.E. Future Prospective and Tasks of WP5

In the coming months of the HighNESS project, the WP5 Team will work on the following tasks:

1. Finalizing the detailed design of the LD_2 moderator, including structural-mechanics and fluid-dynamics simulations, structural materials selection, manufacturability verification, weldability analysis, definition of fluid parameters, cooling process concept design, and integrability.

2. Preliminary design of the He-II UCN source including materials selection, cooling process concept design, and integrability.

3. Manufacturing of ND advanced reflectors for the upcoming experiment at the Budapest moderator test facility. Support in the implementation of the experiment (hydrogen liquefaction, parahydrogen generation, and measurement).

VI. ADVANCED REFLECTORS

The goal of WP6 is to study and optimize the design of advanced neutron reflectors to increase neutron delivery to the instruments. This can be achieved both by wrapping the

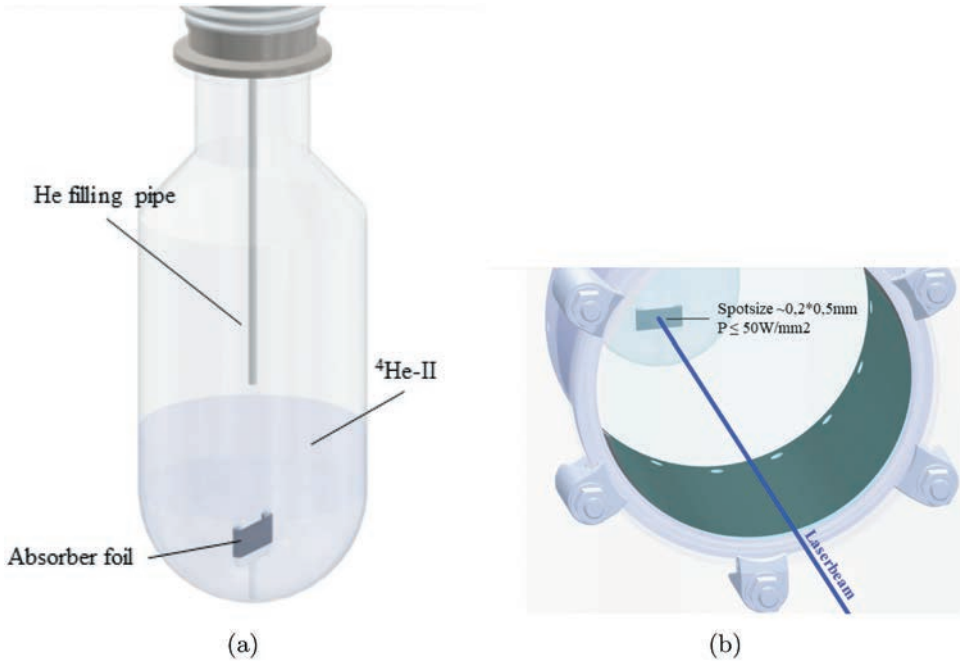

Fig. 20. (a) Glass cryostat with absorber foil filled with He-II. (b) View through the beam port window inside the insulation vacuum vessel with an impinging laser beam.

moderator with CN reflectors, thus increasing the chances for neutrons to get moderated further, and by use of advanced reflectors in the extraction channel to transport more neutrons to the first neutron guide. The findings from WP2 and WP3 for the novel materials, which have been implemented in the related Monte Carlo software (see Sec. II), are essential for the success of this endeavor. A plug-in for NCrystal[47] to describe ND SANS has been developed in collaboration with WP2 to perform the design studies needed in WP6. This plug-in extends the simulation potential of the library by modeling SANS through both empirical models (i.e., fitting existing experimental data) and theoretical models. The capability for directly loading additional experimental data has also been implemented. The most updated version of the code is available with open-source access in the HighNESS GitHub repository.[48] The reliability of the code has been extensively tested in different setups simulated in McStas,[22,23] and the results are comparable with available experimental data. As an example, the reflectometry experiment described in Ref. [49] was reproduced in McStas, and the results are shown in Fig. 21. (The spike in Fig. 21b is caused by the Si window of the sample holder, not included in the simulation).

The simulations capture important features of the real ND powder, despite the lack of more sophisticated physics, like a model for small diamond grains. A more extensive discussion on the topic has been presented in Ref. [10].

As discussed in Sec. V, a dedicated experimental campaign at BNC is being planned and will entail the installation of advanced neutron reflectors both around the moderator and in the extraction channel. The candidates for the first location are MgH_2 and NDs both at room temperature. The differences between these two materials are well highlighted in Ref. [36]. Above 10^{-4} eV, NDs are almost transparent due to predominance of SANS. In the VCN range, instead, NDs' reflectivity rapidly increases to almost 1, even for a small amount of powder. On the other hand, the reflectivity of MgH_2 stays roughly constant around 0.5 in a wide energy range, despite the increasing absorption by hydrogen at lower energies. In the extraction channel, a thin layer of ND powder (e.g., 0.5 cm) is expected to give a significant increase on the CN flux.[50] This is mainly due to the quasi-specular reflectivity feature exhibited by ND in the cold energy range.[51] A sketch of the MCNP model used for this study is shown in Fig. 22, and it is based on the setup of Fig. 18.

VI.A. Future Prospective and Tasks of WP6

In the following months until the end of the project, WP6 will be involved in carrying out the more extensive benchmark for the ND plug-in in the experimental setup relevant to the HighNESS application. Also, the success of the experimental campaign in Budapest will be crucial

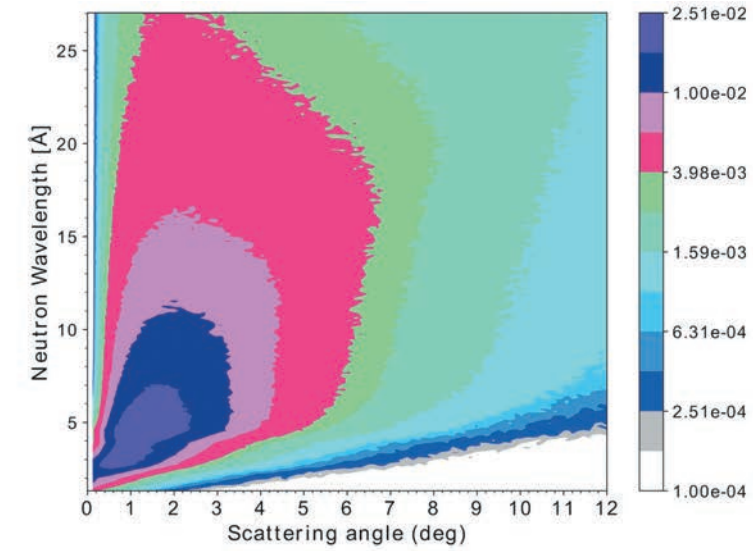

(a)

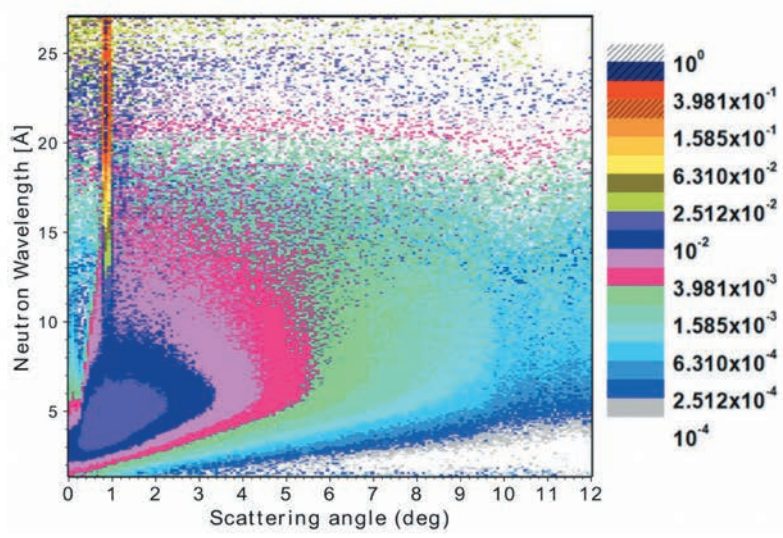

(b)

Fig. 21. (a) Probability of neutron scattering from the surface of fluorinated ND powders as a function of the neutron wavelength and the scattering angle in the McStas simulation with hard sphere model and (b) in Ref. [49]. The neutron incidence angle on the sample is 1°deg. The same color map is adopted for the relevant reflectivity range.

to build confidence in the modeling capabilities for future implementation of advanced reflectors at ESS.

Preliminary simulations using TSL developed within WP2 have shown that a gain factor of about 2 in neutron counts between 4 and 10 Å could be reached at the extraction tube with the combined use of a 1-cm-thick MgH_2 layer around the moderator and only 0.5 cm of NDs around the extraction tube. This experimental campaign will allow for the validation of neutron transport calculations in the presented in-pile environment, thereby building confidence in the modeling capabilities to be used for future implementation of advanced reflectors at ESS.

VII. CONDENSED MATTER SCIENCE

The work carried out in WP7 concerns the definition and the optimization of the conceptual designs for the neutron scattering instruments that will benefit from the second moderator cold source designed in the HighNESS project. The instruments are designed

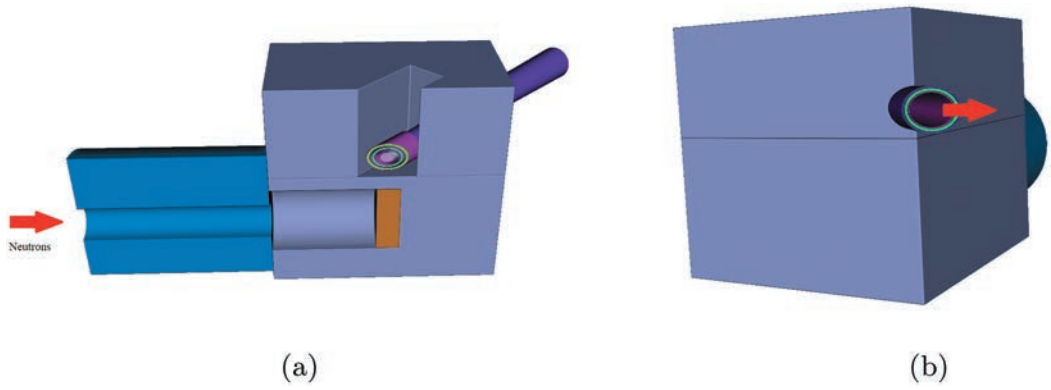

Fig. 22. (a) Side cutaway and (b) downstream 3D view of the MCNP model for the Cold Moderator Test Facility at the BNC based on CAD files[52] with the insertion of the HighNESS reflectors and extraction system. Blue: steel collimator; gray: lead reflector; orange: beryllium disk; pink: liquid para-H_2; green: advanced reflectors; purple: aluminum structure.

considering the potential higher spectral intensity and the gains at longer wavelengths that will be offered by the sources currently under optimization in WP4 (see Sec. IV). The presented conceptual designs in this work include two complete alternative concepts for SANS instrumentation and a conceptual design for a neutron imaging (NI) instrument. A neutron spin-echo instrument design is also being carried out, but since its development is still in the preliminary stage, it will not be described in this paper. The conceptual designs for SANS and NI have reached a state of maturity that enables parametric performance studies in connection with the moderator design development. The performance of the instruments has been tested via Monte Carlo ray-tracing simulations, using McStas,[22,23] as well as q-range and q-resolution calculations. For the overall optimization of the guide systems and optics of the proposed instruments, the software package guide_bot[53] will be used; guide_bot offers a systematic, fast, and flexible solution for optimization processes. For the needs of the HighNESS project, guide_bot is being modified and improved, with respect to its former version,[53] into a Python-based version. Additionally, for the McStas simulations, the WP7 Team has developed components for Wolter optics[54–56] that are also implemented in guide_bot.

VII.A. Small-Angle Neutron Scattering

A SANS instrument, specifically designed to view the lower moderator, offering increased intensity of CNs, will be able to measure with longer wavelengths and access extended q-ranges. As such, we can access larger length scales within samples, potentially overlapping with the length-scale regime of NI without significant loss of flux, which is one of the main concerns of this flux-limited method. Accessing extended length scales and the prospect of using smaller samples could be beneficial to research fields such as structural biology[57] and superconductivity.[58,59] Current efforts to access these length scales, known as very-small-angle neutron scattering or ultra-small-angle neutron scattering, typically suffer from very long counting times and employ elaborate instrument concepts designed to compensate for the very low source brightness of neutrons at long wavelengths. Overall intensity gains will also allow rapid measurements with small beams, and scanning-SANS measurements will thus be possible. Hence, local features and structural variations throughout inhomogeneous samples can be probed. Faster measurements on the other hand, in time-resolved SANS, will enable the study of processes and structural transformations (e.g., reorientation dynamics of anisometric magnetic particles).[60] The generally lower source flux at long wavelengths can be compensated for by employing novel focusing techniques (e.g., Wolter Optics). Wolter optics can offer higher flux at the sample position by collecting a large proportion of the incident neutron beam coming from the moderator surface. Such a concept profits not only from the improved CN flux but also from the large moderator size available at the new moderator.

Based on the above envisioned applications, we have accordingly developed two conceptual designs for SANS, where the first is a conventional instrument drawing on the expected gains in CN intensity. The second concept, on the other hand, attempts to utilize novel Wolter focusing optics to additionally fully benefit from the larger moderator surface. The first SANS instrument is designed based on a conventional small-angle neutron scattering (ConvSANS) geometry, with the use of a typical pinhole

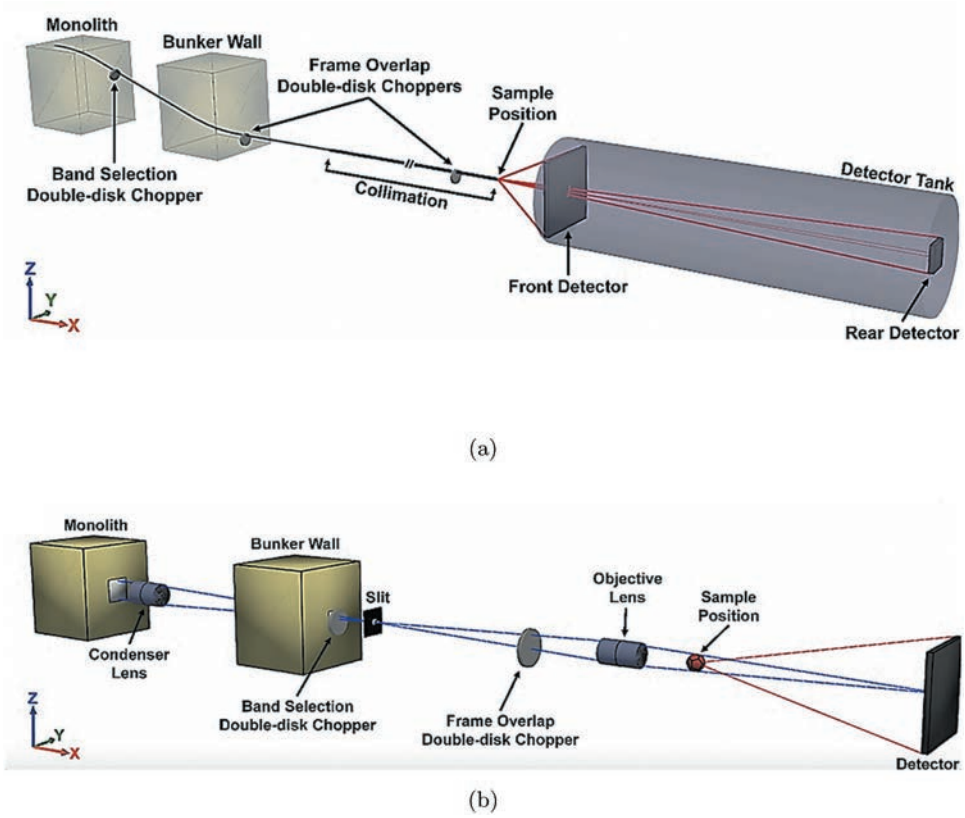

Fig. 23. (a) ConvSANS instrument layout and (b) WOF-SANS instrument layout. In both (a) and (b), the red lines represent scattered neutrons with maximum scattering angles at the edges of each detector. In (b) the blue lines represent the focused neutron beam by the Wolter optics.

collimator. An overview of the instrument can be seen in Fig. 23a.

The collimation maximum length is 30 m, with sample-to-detector distances of 3 m (wide angles) and 30 m (small angles) and a total instrument length of 80 m. The long collimation offers high angular resolution, which is also complemented by the high wavelength resolution due to the instrument length. Two benders, one through the monolith wall and another one through the bunker wall, are used as short-wavelength cutoff filters and provide twice out-of-line-of-sight curvature to minimize the spallation background reaching the detector area. The current conceptual design assumes the guide size to be 3 $\times$ 3 cm throughout the whole instrument. A bandwidth double-disk chopper is placed in the in-bunker section of the instrument, at 6.5 m from the moderator. An additional pair of choppers is placed just beyond the bunker wall, at 15 m, to suppress frame overlapping. The detector configuration employed for the current setup is based on a "window-frame" design. The front detector, 53 m from the moderator, has a 3 $\times$ 3-m surface area with a 0.1 $\times$ 0.1-m window opening at the center. The rear detector is located at 80 m from the moderator and has a 1 $\times$ 1-m surface area.

A Wolter focusing optics small-angle neutron scattering (WOF-SANS) instrument makes use of a pair of Type I Wolter optics[61] to take advantage of the large moderator surface and to increase the neutron flux at the sample position. A schematic of the current instrument design can be seen in Fig. 23b. The first Wolter optics system is used as a condenser lens, and it is in the in-bunker section of the instrument, 6.5 m from the moderator. It consists of 10 nested paired parabolic and hyperbolic sections, currently 25 cm in length each, and has a focal length of 15 m. At the focal point, 21.5 m from the moderator, a circular aperture of 4 mm in diameter is used to suppress any out-of-focus rays and any neutrons that pass through the condenser without reflecting. The second Wolter optics system is used as an objective lens. It is located 31.5 m from the moderator, and it has symmetric focal lengths, aperture-to-objective and objective-to-detector, of 10 m each, with a magnification $M = 1$. As such, the focused beam spot

size on the detector center is expected to be 4 mm in diameter. The objective lens consists of 10 nested paired elliptical and hyperbolic (E-H) sections, also 25 cm in length each. The position sensitive detector is considered to have a surface area of 3 × 3 m and is placed at a fixed position matching the common focus of the E-H mirrors, 41.5 m from the moderator.

For both instruments, initial evaluation of their performance was performed by calculating the q-ranges and corresponding q-resolutions, aiming to reach q-values below 10^{-3} Å^{-1}. To do so, reasonable wavelength bands were chosen based on each instrument's available wavelength bandwidths (3.5 and 6.8 Å, respectively, when operating with the 14-Hz source frequency). For ConvSANS, we used a 3-cm-diameter source aperture and a 1.5-cm-diameter sample aperture and assumed a pixel size of 1 cm. For the WOF-SANS, we used a source aperture of 4-mm diameter and a pixel size of 4 mm. For both instruments, we chose a minimum wavelength of 7.2 Å. The results are given in Fig. 24.

For further evaluation of the instruments' performance, we have done Monte Carlo ray-tracing simulations using McStas.[22,23] For the simulations, we used an MCPL[62] input file (MCPL is a binary format storing information on the state of a particle (momentum and position) and allows for interchanging of trajectories, particles, or entire events over different Monte Carlo–based simulation programs) as a source, corresponding to the lower moderator design with a viewable area of 15 × 15 cm^2. Figure 25 shows the resulting wavelength spectra, for both instruments, at the corresponding sample positions, with the WOF-SANS configuration having significant gains in total neutron intensity at the sample.

VII.B. Neutron Imaging

Neutron imaging is a rapidly evolving real space technique probing macroscopic structures with a very wide range of applications covering both academic research and areas with direct industrial impact. An imaging instrument viewing the second moderator could provide enhanced performance in a complementary regime of applications with respect to the under-construction ODIN instrument,[63] in particular, for large industrial samples. The large viewable area of the moderator will allow for a larger and potentially more uniform field of view while the expected higher intensity in wavelengths above 5 Å can greatly increase, for example, the sensitivity of polarized NI, extending the range of accessible three-dimensional (3D) magnetic field distributions to lower fields and local electric currents. The long-wavelength regime will also greatly improve quantitative high-resolution imaging with neutrons, as the signal is not affected by diffraction, which is otherwise unavoidable from some structural materials.

Accordingly, the NI instrument is designed based on a conventional NI pinhole geometry, which enables optimum beam homogeneity. The total length of the instrument is not fixed; however, it will be kept rather short. A short instrument will not require a neutron guide and therefore will profit from a more uniform beam, which is essential for the best image quality. With the use of a movable sample-detector configuration, the length can be adapted, and along with adjusting the size of the pinhole, resolution, size, and flux can be traded flexibly. With the large homogeneous field of view, high intensity, and only very moderate wavelength resolution, the instrument will well complement the currently constructed instrument ODIN at ESS. A schematic of the NI instrument can be seen in Fig. 26.

In the above setup, we can define the L/D ratio with L being the distance between the aperture and the sample and D the aperture diameter. This ratio gives the geometric resolution of the configuration as it determines the image blur, $d = l/(L/D)$, in the detector plane, where l is the distance between the sample and the detector. With L = 16 m and D = 3 cm, L/D = 533.3. This can be further improved by either reducing the aperture size or increasing L. However, experimental, and thus resolution, adjustments should be made considering implications on flux and vice versa. Simulations with different L/D were performed using McStas, using the same source MCPL file as for the SANS instruments. Selected examples of resulting fields of view are given in Fig. 27.

VIII. FUNDAMENTAL PHYSICS

In WP8, the possibilities of the high-intensity neutron source for experiments in fundamental physics are investigated. The work is mostly dedicated to the design of the NNBAR experiment.[4] This experiment would exploit the neutron flux available from the newly designed lower moderator to search for the baryon number violating process of a neutron n converting to an antineutron $\overline{n}$. A key aim is to obtain a sensitivity that is three orders of magnitude greater than the one achieved in the last search with free neutrons.[64] The experiment comprises neutron focusing and transport in a magnetically shielded region to a carbon target that is surrounded by a detector that can observe the annihilation between an antineutron and

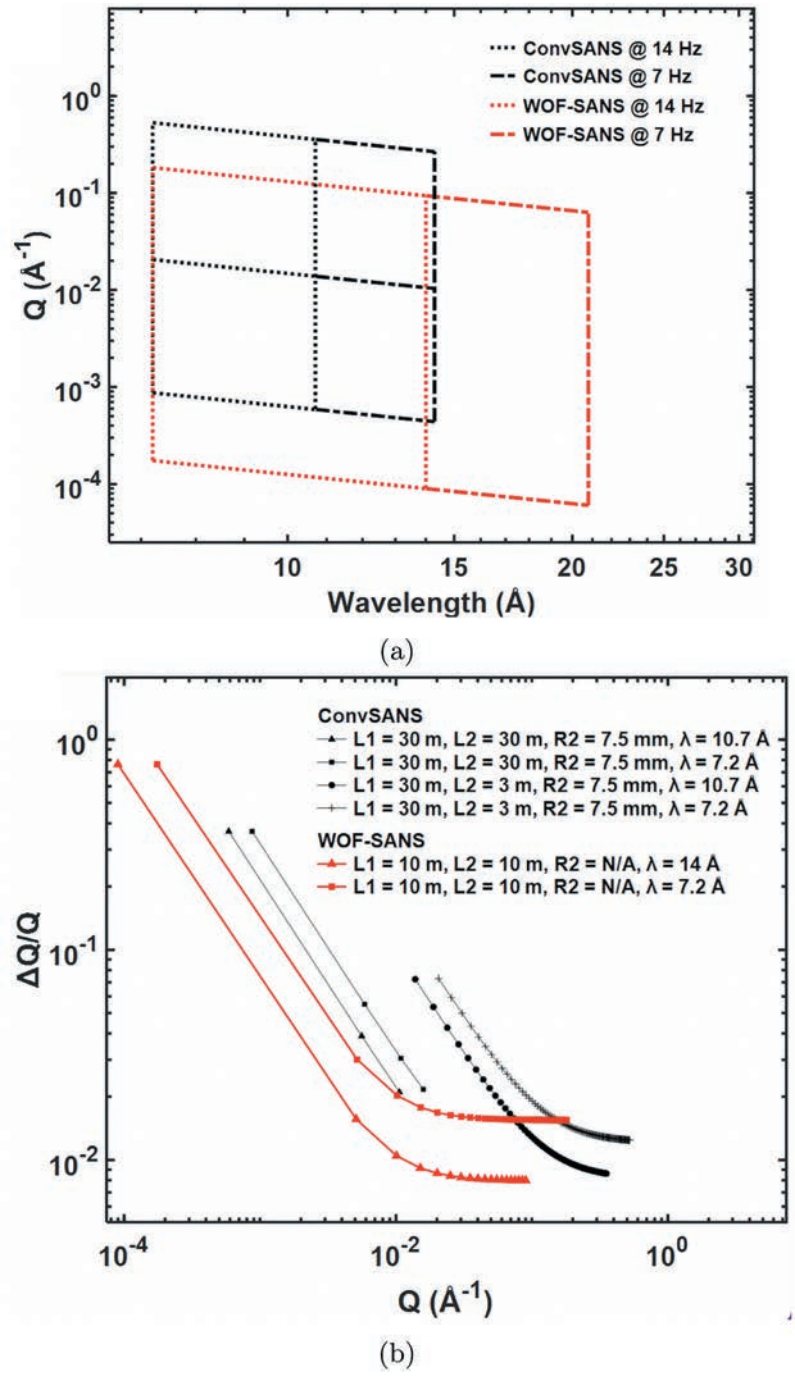

Fig. 24. (a) The q-ranges as a function of wavelength for ConvSANS and WOF-SANS, calculated using a minimum wavelength of 7.2 Å and for both 14- and 7-Hz modes of operation. (b) The q-resolution as a function of scattering vector q.

a target nucleon. The antineutrons will annihilate and will be detected via their multipion and photon decay signature.

VIII.A. Overview of Experiment and Reflectors

In Fig. 28, a schematic of the planned experimental setup of the NNBAR experiment at ESS is shown. Neutrons leave the moderator and traverse the LBP, which was specially designed for the NNBAR experiment. The LBP covers three regular ESS beam ports, corresponding to a size of 105×70 cm^2 at a distance of 2 m from the moderator. It will thus allow the NNBAR experiment to use a large fraction of the solid angle, leading to a high intensity of the CN beam. A reflector is placed in the region behind the LBP's exit to focus the

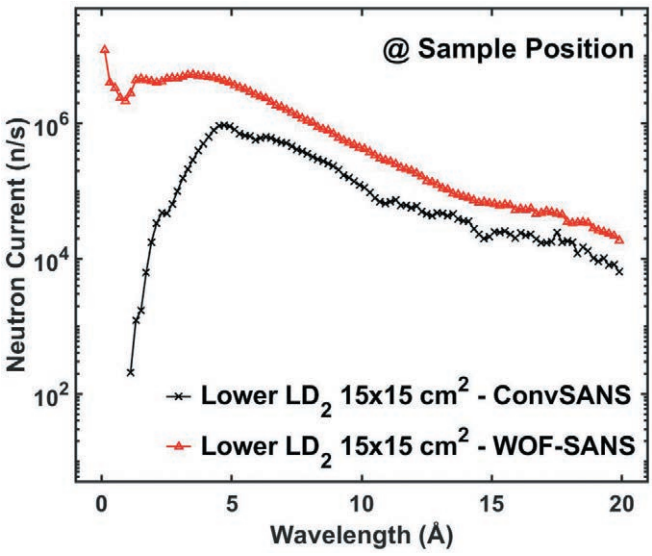

Fig. 25. Wavelength spectra at the sample position, as simulated with McStas, for ConvSANS and WOF-SANS.

neutrons in the direction of the detector located upstream. Having passed the optics, neutrons travel in a magnetic field–free region toward a distant carbon target. The target is surrounded by a detector to observe a baryon number annihilation signal of an antineutron with a nucleon in a carbon nucleus. The moderator-to-detector distance is foreseen to be 200 m.

An option for the reflector that is considered in the project is in a nested arrangement of neutron mirrors as proposed in Refs. [46] and [65]. The arrangement utilizes the general property of an elliptical-shaped mirror where rays that are sent out from the first focal point are reflected to the second one. If the outer layer of such nested elliptical guides is given, the inner layers can be constructed in a recursive manner such that the layers will not shadow themselves. In the sketch of Fig. 29, the principle is shown. A straight line from the source position M to the end of the optics from the layer with index n defines the optimal starting position of the next layer $n + 1$.

Different layouts of the nested reflectors that are symmetrical around the axis-in-flight direction are possible. These are (a) a mono planar system, (b) a double planar system, and (c) a cylindrical system. In Fig. 30, 3D renderings of the different types are shown.

To simulate the transport capabilities of the different reflector geometries, a method for an automated creation of the components has been developed. From a set of given parameters (focal distance, starting point, length, etc.) that define the geometric constraints, the components are generated and can be used in McStas[22,23] simulations.

An alternative to the elliptical-shaped reflectors are Wolter optics[61] systems. These are a full family of mirror layouts and consist in the case of our application of two segments in a hyperbolic and elliptical shape. The segments are constructed in a way so that they fulfill the Abbé sine condition[66] in good approximation. Such optics produce sharp and aberration-free images. Their suitability for an NNBAR experiment will be studied in the next months of the HighNESS project.

VIII.B. Beamline Simulations

While the LBP is of fundamental importance for reaching the sensitivity goals of the NNBAR experiment, it will also transport a large number of fast neutrons and spallation background beyond the target monolith. The NNBAR beamline will therefore have to be heavily shielded, especially the first few meters exterior to the target monolith. This includes reinforcement of the bunker roof in the region around the NNBAR beamline as well as additional shielding inside the bunker.

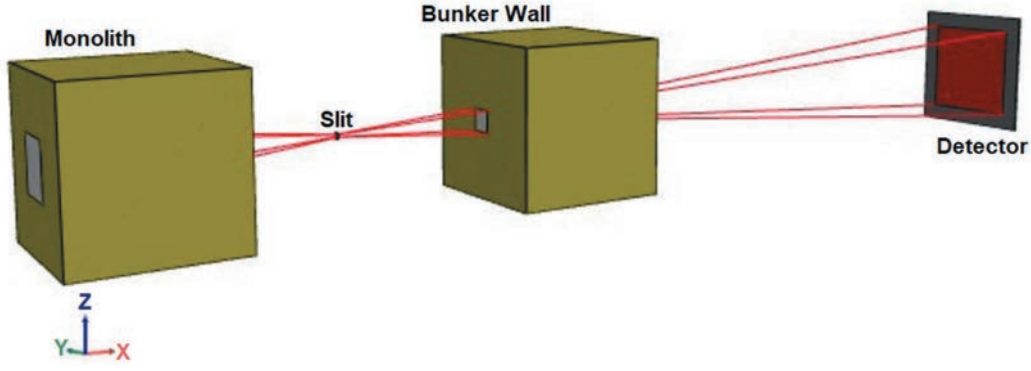

Fig. 26. Neutron imaging instrument layout.

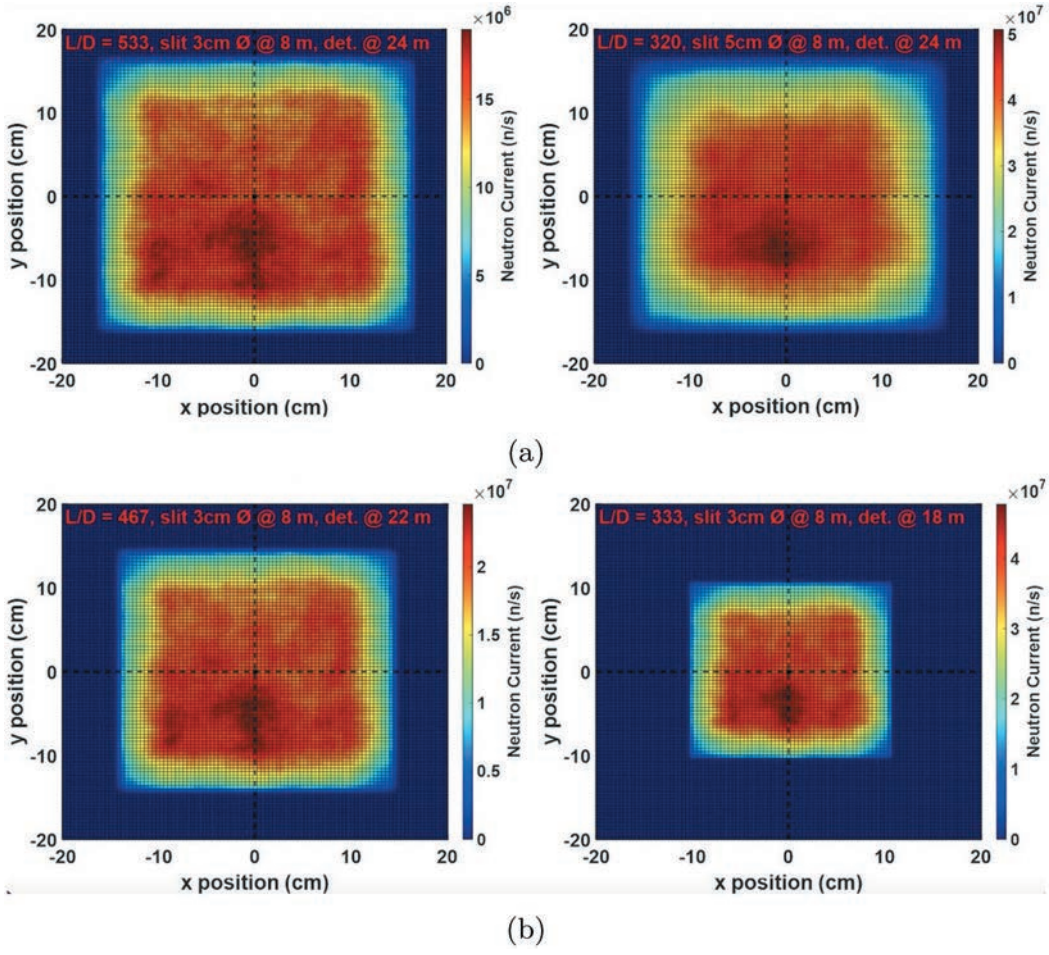

Fig. 27. Detector images from Monte Carlo ray-tracing simulations for different L/D (a) by either changing the aperture size with constant detector distance or (b) by changing the detector distance with constant aperture size.

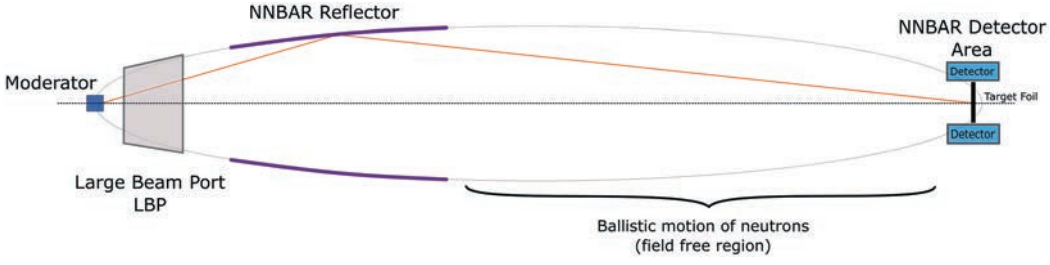

Fig. 28. Schematic of the NNBAR experiment (not in scale). The moderator-to-detector distance is foreseen to be 200. The annihilation target is of radius 1m. Vacuum tube and magnetic shielding are not shown.

To investigate the amount of additional shielding needed inside the bunker, a model of the NNBAR beamline was created using the CombLayer software package.[67] CombLayer allows for the production of geometries suitable for several radiation codes such as PHITS or MCNP. In this case, simulations were carried out using MCNP6.2.[68] The MCNP model is shown in Fig. 31a. Apart from NNBAR itself, the neighboring HEIMDAL[69] beamline was also included. Figure 31b shows a simulated dose map without additional shielding of the NNBAR beamline. In this case, the dose rate in the proximity of the beamline exceeds 100 Sv/h. This not

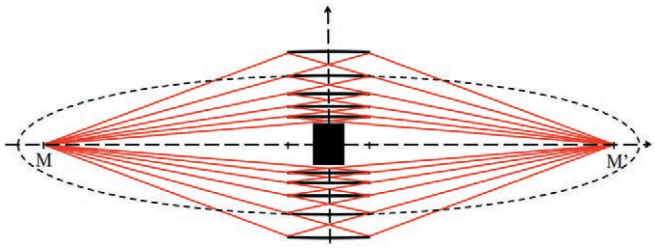

Fig. 29. Schematic of elliptically shaped neutron mirrors in a nested arrangement. M and M' are the common focal points of the ellipses that form the individual layers.

only would be a problem for experiments at neighboring beamlines but also exceeds the dose rates that the bunker walls have been designed for. However, as shown in Fig. 31c, 40-cm-thick walls of heavy concrete are sufficient to reduce the dose rate to ≈ 1 Sv/h, which is the level of radiation emitted inside the bunker by the standard ESS neutron scattering instruments (as shown in Fig. 31c where the radiation emitted by the HEIMDAL instrument is around few Sv/h). Additional beamline simulations are currently under preparation, including simulations of the bunker roof and the NNBAR guide shielding outside the bunker. For variance reduction, these simulations will make use of a specially developed sampling method based on probability density evaluation and duct-source biasing.[70] This will allow for the completion of these simulations with high statistics while preserving correlations between positions, angles, and energies of neutrons emerging from the LBP.

VIII.C. Beam-Induced Background in Detector

The background coming from the LBP will also be a challenge for the NNBAR detector. While the principal background for the last search with free neutrons was caused by cosmic rays,[64] the search also observed substantial beam-induced background that required mitigation efforts to suppress. Lithium plates were deployed around the experimental area to absorb neutrons. An important irreducible background arose from gammas produced from neutron capture at the carbon target.

A Geant-based framework has been developed to study beam-induced backgrounds in the NNBAR experiment. The detector and general software framework of the experiment are described elsewhere.[71–72] The

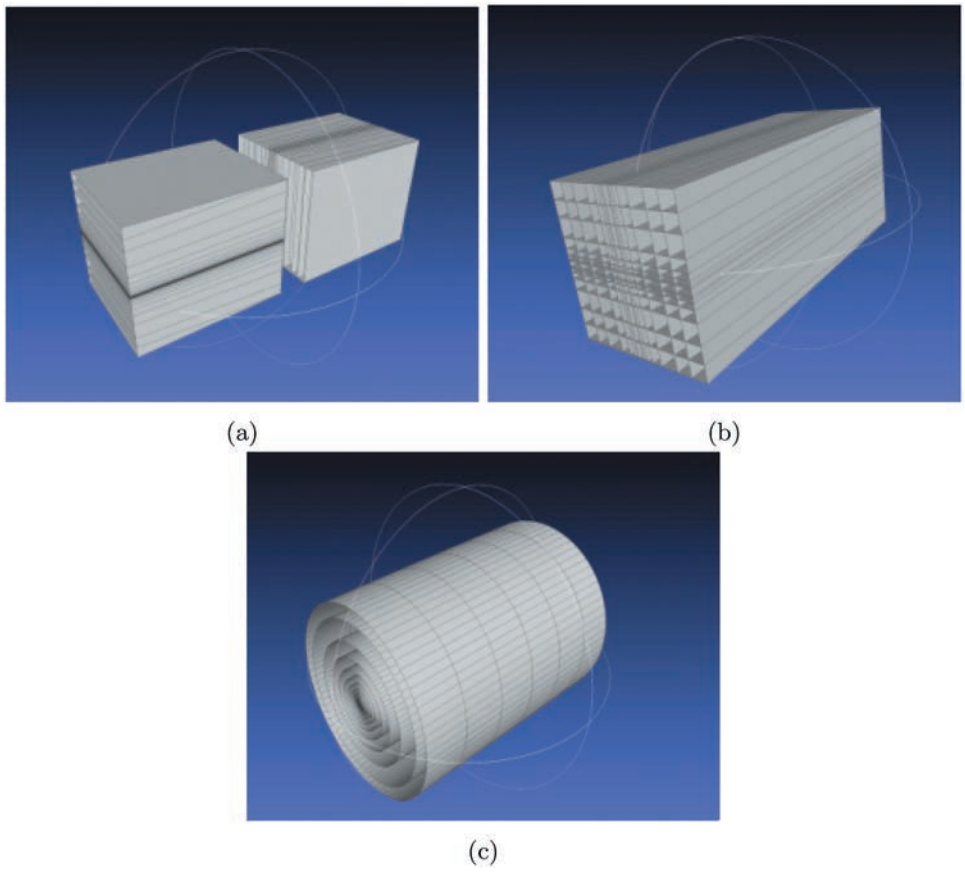

Fig. 30. Types of nested optical components: (a) mono planar, (b) double planar, and (c) cylindrical.

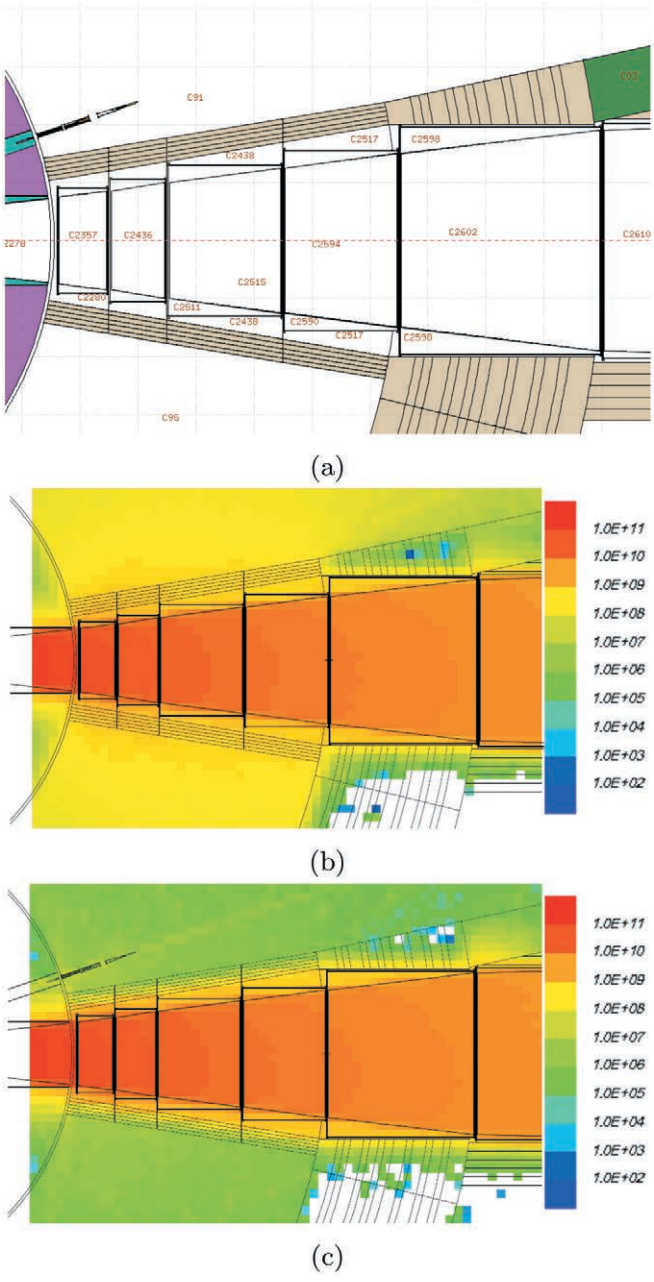

Fig. 31. (a) Model of NNBAR beamline created in CombLayer. (b) Dose map from MCNP simulation of NNBAR beamline without additional shielding. (c) Dose map from MCNP simulation of NNBAR beamline with 40 cm of heavy concrete as additional shielding. Dose rates are given in μSv/h.

detector comprises tracking, silicon along with a time projection chamber, a scintillator, and lead-glass calorimeter.

A weighted sample of around 440 000 simulated neutrons, as focused by differential reflectors[5] and that arrive at the detector area, has been studied. Figure 32 shows the properties of neutrons arriving at the detector area at a distance of around 195 m from the reflector and that are further propagated to the carbon target at 200 m. The data were split into eight simulated pulses. To match the region in which the reflecting simulation is reliable, a kinetic energy of less than 0.1 eV is taken. The plots show the buildup of a flat, pulse-independent asymptotic region of slow neutrons.

A key concern in the design of the experiment is the flux of photons from neutron capture and inelastic scattering at the carbon target and the surrounding infrastructure (e.g., beam pipe). In addition to providing a continuous low-energy "pile-up" background, in the worst case, this can mimic the signature of an antineutron annihilating in the target. Mitigation efforts must therefore be taken. A full optimization of neutron absorption and background suppression options is being undertaken. An example of this is the coating of the insides of the beam pipe with neutron absorber plates. Figure 33 shows the intensity (number of photons per millisecond) exiting the beam pipe and entering the detector for the case where no absorber coating is used and a coating with ^{6}Li is used. As the plots show, the photon yield is substantially reduced.

IX. COMPUTING INFRASTRUCTURE

The objectives of WP9 are to provide the required scientific computer infrastructure for the simulations needed in the HighNESS project and to offer the tools developed available as cloud resources. Two simulation software packages need to be provided, namely, McStas and NCrystal, for thermal neutron transport.

In the first 2 years of the HighNESS project, the focus has been on providing computational resources for the participants, providing the functionality required. This has taken the form of (1) on-boarding users from the HighNESS community on the ESS Data Management and Software Center (DMSC) scientific compute cluster, (2) providing storage capacity on the ESS scientific computer systems for HighNESS relevant data, (3) keeping the McStas software up to date on the ESS DMSC scientific computer cluster, and (4) enabling the possibility for running Jupyter notebooks as a batch job on the DMSC computer cluster. Aside from providing basic computational capacities for the HighNESS project, an effort has been undertaken to develop a proof-of-concept cloud solution for McStas simulation

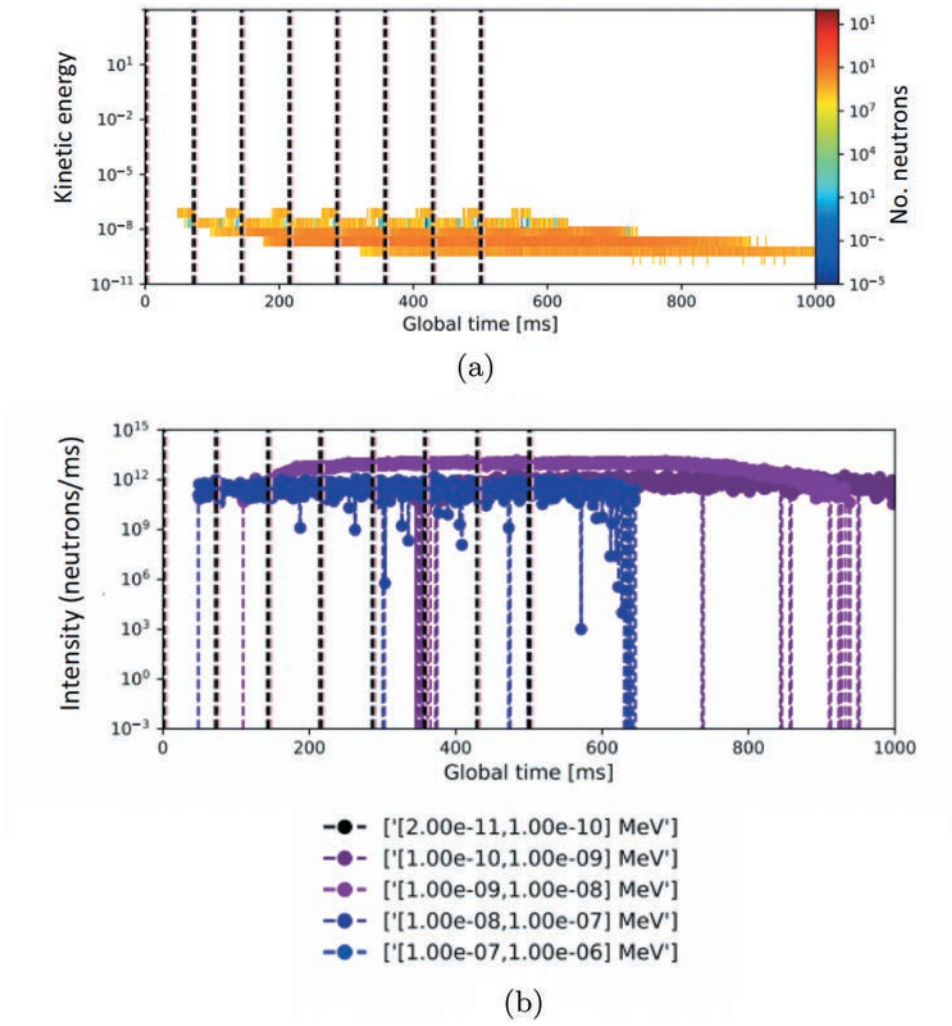

Fig. 32. (a) Kinetic energy versus arrival time. (b) Intensity (number of neutrons per second) versus arrival time. The dashed vertical lines represent the reset of the ESS clock.

using JupyterHub. This has been achieved by utilizing a service put in place as part of the PaNOSC[c] project, namely, the e-learning platform pan-learning.org. In pan-learning.org, a training course can encompass the possibilities for performing limited-size McStas simulations, and a special course has been set up for HighNESS providing the possibility for HighNESS users to perform such simulations proving the viability of using JupyterHub as a framework for the cloud services to be provided. Such JupyterHubs must be provided as a more independent service than what is available in the pan-learning platform and need to be connected to sufficient computational capacities, which is not the case for pan-learning at moment.

[c] 2Photon and Neutron Open Science Cloud https://www.panosc.eu/.

X. CONCLUSION

In summary, in the first 2 years of the HighNESS project, many results have been achieved in the different WPs. Thanks to the work carried out in WP2, WP3, and WP6, it is now possible to use advanced reflector materials in the neutronic simulations of the HighNESS moderators. The neutronic design of the CN source has been finalized by WP4, and it is now being studied by the engineering work package (WP5). Several designs for the UCN sources are now under evaluation as well as options for a VCN source. Different neutron scattering instrument concepts have been proposed by WP7. For fundamental physics, the NNBAR optics system has been designed, and background studies are currently being carried out. Several developments are still ongoing and will be part of the Conceptual Design of

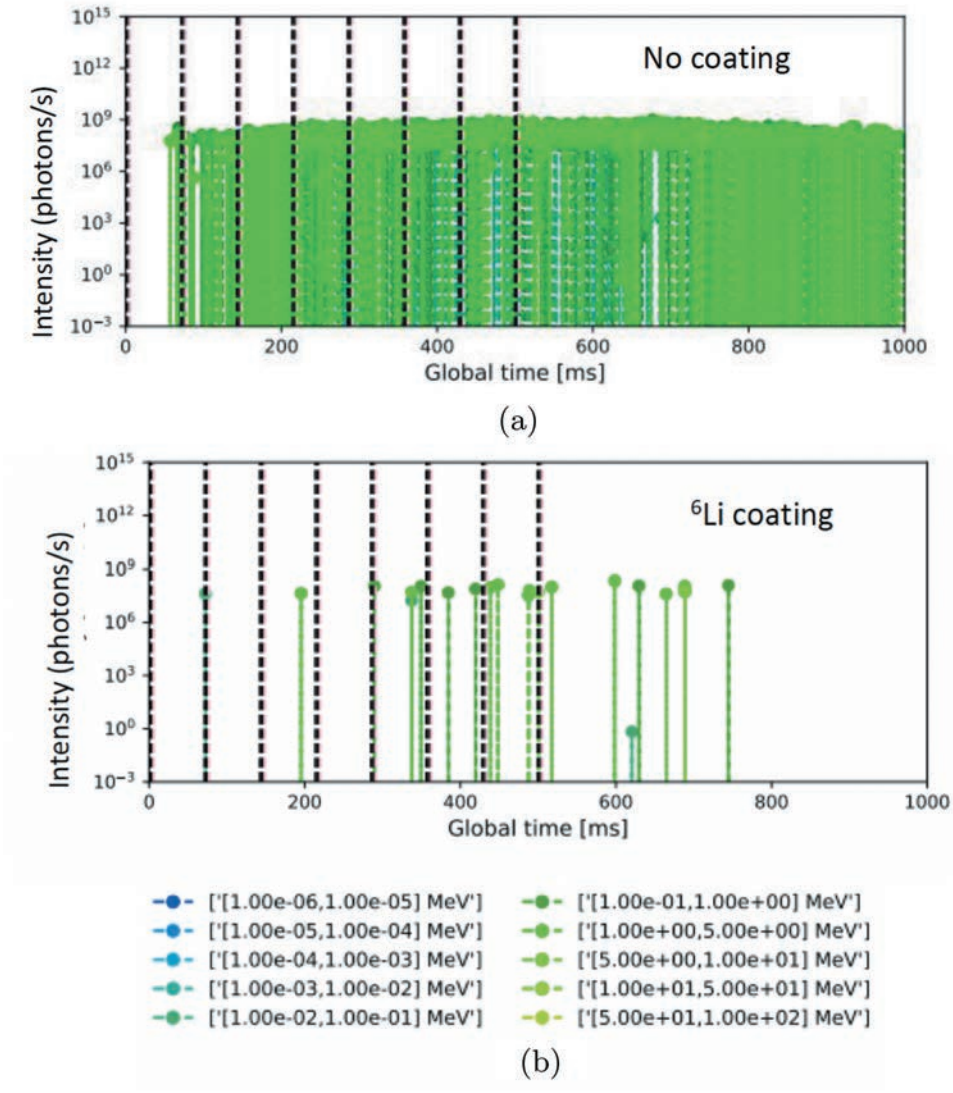

Fig. 33. The intensity of photons (number of photons per millisecond) entering the detector. (a) No coating of the detector area. (b) Coating with ^{6}Li. The dashed vertical lines represent the reset of the ESS clock.

the ESS upgrade, which is the final objective of the HighNESS project.

Acronyms

BNC: Budapest Neutron Center
CN: cold neutron(s)
ConvSANS: conventional small-angle neutron scattering
DMSC: Data Management Software Center
DOS: density of states
E-H: elliptical and hyperbolic
ESS: European Spallation Source
FOM: figure of merit
He-II: superfluid helium
ILL: Institut Laue-Langevin
LBP: Large Beam Port
LD_2: liquid deuterium
MCB: moderator cooling block
ND: nanodiamond (particles)
NI: neutron imaging
NNBAR: neutron-antineutron oscillation experiment
PSI: Paul Scherrer Institut
SANS: small-angle neutron scattering

SD_2: solid ortho-deuterium
TDF: deuterated tetrahydrofuran
THF: tetrahydrofuran
ToF: time of flight
TSL: thermal scattering libraries
UCN: ultracold neutron(s)
VCN: very cold neutron(s)
WOF-SANS: Wolter focusing optics small-angle neutron scattering
WP: work package
WP1: Work Package 1
WP2: Work Package 2
WP3: Work Package 3
WP4: Work Package 4
WP5: Work Package 5
WP6: Work Package 6
WP7: Work Package 7
WP8: Work Package 8
WP9: Work Package 9
WP10: Work Package 10
3D: three-dimensional

Funding

This work was supported by the HighNESS project and is funded by European Commission (H2020-951782).

Disclosure Statement

No potential conflict of interest was reported by the author(s).

ORCID

V. Santoro http://orcid.org/0000-0001-5379-8771
A. Chambon http://orcid.org/0000-0002-3733-3226
T. Kittelmann http://orcid.org/0000-0002-7396-4922
B. Lauritzen http://orcid.org/0000-0001-7173-1650
N. Rizzi http://orcid.org/0000-0003-1542-1695

References

1. L. ZANINI et al., "Design of the Cold and Thermal Neutron Moderators for the European Spallation Source," *Nucl. Instrum. Methods Phys. Res., Sect. A*, **925**, 33 (2019); http://dx.doi.org/10.1016/j.nima.2019.01.003.
2. V. SANTORO et al., "Development of High Intensity Neutron Source at the European Spallation Source," *J. Neutron Res.*, **22**, *2–3*, 209 (2020); https://doi.org/10.3233/JNR-200159.
3. V. SANTORO, "The HighNESS Project and Future Free Neutron Oscillations Searches at the ESS," *Proc. European Physical Society Conf. High Energy Physics*, Online Conference, July 26–30, 2021, EPS-HEP2021, *Proceedings of Science*, p. 711 (2022); https://doi.org/10.22323/1.398.0711.
4. A. ADDAZI et al., "New High-Sensitivity Searches for Neutrons Converting into Antineutrons and/or Sterile Neutrons at the HIBEAM/NNBAR Experiment at the European Spallation Source," *J. Phys. G*, **48**, *7*, 070501 (2021); https://doi.org/10.1088/1361-6471/abf429.
5. F. BACKMAN et al., "The Development of the NNBAR Experiment," *J. Instrum.*, **17**, *10*, P10046 (2022); https://doi.org/10.1088/1748-0221/17/10/P10046.
6. R. MACFARLANE and A. KAHLER, "Methods for Processing ENDF/B-VII with NJOY," *Nucl. Data Sheets*, **111**, *12*, 2739 (2010); http://www.sciencedirect.com/science/article/pii/S0090375210001006.
7. K. RAMIĆ et al., "NJOY+NCrystal: An Open-Source Tool for Creating Thermal Neutron Scattering Libraries with Mixed Elastic Support," *Nucl. Instrum. Methods Phys. Res., Sect. A*, **1027**, 166227 (2022); https://www.sciencedirect.com/science/article/pii/S0168900221010755.
8. X.-X. CAI and T. KITTELMANN, "NCrystal: A Library for Thermal Neutron Transport," *Comput. Phys. Commun.*, **246**, 106851 (2020); https://www.sciencedirect.com/science/article/pii/S0010465519302280.
9. P. K. ROMANO et al., "OpenMC: A State-of-the-Art Monte Carlo Code for Research and Development," *Ann. Nucl. Energy*, **82**, 90 (2015); https://www.sciencedirect.com/science/article/pii/S030645491400379X.
10. N. RIZZI et al., "Benchmarking of the NCrystal SANS Plugin for Nanodiamonds," *Proc. 14th Int. Topl. Mtg. Nuclear Applications of Accelerators*, Washington D.C., November 30–December 4, 2021, p. 67, American Nuclear Society (2021).
11. K. RAMIC et al., "Advances in Nuclear Data and Software Development for the HighNESS Project," *Proc. 14th Int. Topl. Mtg. Nuclear Applications of Accelerators*, Washington D.C., November 30–December 4, 2021, p. 78, American Nuclear Society (2021).

12. D. D. DIJULIO et al., "Thermal Scattering Libraries for Cold and Ultra-Cold Neutron Reflector Materials," *Proc. 15th Int. Conf. Nuclear Data for Science and Technology (ND2022)*, Virtual Conference, July 21–29, 2022; https://doi.org/10.1051/epjconf/202328417013

13. J. LIU et al., "Ab Initio Study of the Molecular Hydrogen Occupancy in Pure H_2 and Binary H_2-THF Clathrate Hydrates," *Int. J. Hydrogen Energy*, **42**, *27*, 17136 (2017); https://www.sciencedirect.com/science/article/pii/S0360319917322899.

14. A. LENZ and L. OJAMÄE, "Structures of the I-, II- and H-Methane Clathrates and the Ice-Methane Clathrate Phase Transition from Quantum-Chemical Modeling with Force-Field Thermal Corrections," *J. Phys. Chem. A*, **115**, *23*, 6169 (2011); https://doi.org/10.1021/jp111328v.

15. J. P. PERDEW, K. BURKE, and M. ERNZERHOF, "Generalized Gradient Approximation Made Simple," *Phys. Rev. Lett.*, **77**, *18*, 3865 (1996); https://link.aps.org/doi/10.1103/PhysRevLett.77.3865.

16. S. GOEDECKER, M. TETER, and J. HUTTER, "Separable Dual-Space Gaussian Pseudopotentials," *Phys. Rev. B*, **54**, *3*, 1703 (1996); https://link.aps.org/doi/10.1103/PhysRevB.54.1703.

17. S. GRIMME et al., "A Consistent and Accurate Ab Initio Parametrization of Density Functional Dispersion Correction (DFT-D) for the 94 Elements H-Pu," *J. Chem. Phys.*, **132**, *15*, 154104 (2010); https://aip.scitation.org/doi/10.1063/1.3382344.

18. T. D. KÜHNE et al., "CP2K: An Electronic Structure and Molecular Dynamics Software Package—Quickstep: Efficient and Accurate Electronic Structure Calculations," *J. Chem. Phys.*, **152**, *19*, 194103 (2020); https://aip.scitation.org/doi/10.1063/5.0007045.

19. A. TOGO and I. TANAKA, "First Principles Phonon Calculations in Materials Science," *Scr. Mater.*, **108**, 1 (2015); https://doi.org/10.1016/j.scriptamat.2015.07.021.

20. X.-X. CAI et al., "Rejection-Based Sampling of Inelastic Neutron Scattering," *J. Comput. Phys.*, **380**, 400 (2019); https://www.sciencedirect.com/science/article/pii/S0021999118307885.

21. T. KITTELMANN and X.-X. CAI, "Elastic Neutron Scattering Models for NCrystal," *Comput. Phys. Commun.*, **267**, 108082 (2021); https://www.sciencedirect.com/science/article/pii/S0010465521001946.

22. P. K. WILLENDRUP and K. LEFMANN, "McStas (I): Introduction, Use, and Basic Principles for Ray-Tracing Simulations," *J. Neutron Res.*, **22**, *1*, 1 (2020); https://arxiv.org/abs/2010.00318.

23. P. K. WILLENDRUP and K. LEFMANN, "McStas (ii): An Overview of Components, Their Use, and Advice for User Contributions," *J. Neutron Res.*, **23**, *1*, 7 (2021); https://doi.org/10.3233/JNR-200186.

24. O. ZIMMER, "Neutron Conversion and Cascaded Cooling in Paramagnetic Systems for a High-Flux Source of Very Cold Neutrons," *Phys. Rev. C*, **93**, 035503 (2016); https://link.aps.org/doi/10.1103/PhysRevC.93.035503.

25. XuShuqi7/ncplugin-MagScat website; https://github.com/XuShuqi7/ncplugin-MagScat (accessed June 30, 2022).

26. J. M. CARPENTER and B. J. MICKLICH, *Proceedings of the Workshop on Applications of a Very Cold Neutron Source* (2005); https://www.osti.gov/biblio/1248367.

27. V. NESVIZHEVSKY, "Why Very Cold Neutrons Could Be Useful for Neutron Antineutron Oscillation Searches," *J. Neutron Res.*, **24**, 223 (2022); https://doi.org/10.3233/JNR-220003.

28. F. M. PIEGSA, "New Concept for a Neutron Electric Dipole Moment Search Using a Pulsed Beam," *Phys. Rev. C*, **88**, *4*, 045502 (2013); https://link.aps.org/doi/10.1103/PhysRevC.88.045502.

29. F. M. PIEGSA and G. PIGNOL, "Limits on the Axial Coupling Constant of New Light Bosons," *Phys. Rev. Lett.*, **108**, 181801 (2012); https://link.aps.org/doi/10.1103/PhysRevLett.108.181801.

30. A. K. SUM, C. A. KOH, and E. D. SLOAN, "Clathrate Hydrates: From Laboratory Science to Engineering Practice," *Ind. Eng. Chem. Res.*, **48**, *16*, 7457 (2009); https://doi.org/10.1021/ie900679m.

31. F. ROSSI, M. FILIPPONI, and B. CASTELLANI, "Investigation on a Novel Reactor for Gas Hydrate Production," *Appl. Energy*, **99**, 167 (2012); https://doi.org/10.1016/j.apenergy.2012.05.005.

32. W. X. PANG et al., "Experimental Study on the Scale-Up Effect of Gas Storage in the Form of Hydrate in a Quiescent Reactor," *Chem. Eng. Sci.*, **62**, *8*, 2198 (2007); http://www.sciencedirect.com/science/article/pii/S0009250907000516.

33. H. CONRAD et al., "Inelastic Scattering and Spectral Measurements of Advanced Cold Moderator Media," *Physica B*, **350**, *1–3*, Supplement, E647 (2004); https://www.sciencedirect.com/science/article/pii/S0921452604003898.

34. K. H. BECKURTS and K. WIRTZ, *Neutron Physics*, Springer, Berlin (1964).

35. J. R. GRANADA, "Neutron Scattering Kernel for Solid Deuterium," *Europhys. Lett.*, **86**, *6*, 66007 (2009); https://iopscience.iop.org/article/10.1209/0295-5075/86/66007.

36. J. R. GRANADA, J. I. M. DAMIÁN, and C. HELMAN, "Studies on Reflector Materials for Cold Neutrons," *EPJ Web Conf.*, **231**, 04002 (2020); https://www.epj-conferences.org/articles/epjconf/abs/2020/07/epjconf_ucans82020_04002/epjconf_ucans82020_04002.html.

37. F. OTT, "Opportunities in the Use of Very Cold Neutrons in Reflectometry Techniques," *Proc. Workshop Very Cold and*

Ultra Cold Neutron Sources for ESS, Virtual Workshop, February 2–4, 2022.

38. F. MEZEI, "Very Cold Neutrons in Condensed Matter Research," *Proc. Workshop Very Cold and Ultra Cold Neutron Sources for ESS*, Virtual Workshop, February 2–4, 2022.
39. L. ZANINI et al., "Very Cold and Ultra Cold Neutron Sources for ESS," *Proc. Workshop Very Cold and Ultra Cold Neutron Sources for ESS*, Virtual Workshop, February 2–4, 2022.
40. P. SCHMIDT-WELLENBURG, K. ANDERSEN, and O. ZIMMER, "Ultra Cold Neutron Production by Multiphonon Processes in Superfluid Helium Under Pressure," *Nucl. Instrum. Methods Phys. Res., Sect. A*, **611**, *2*, 259 (2009); https://www.sciencedirect.com/science/article/pii/S0168900209015393.
41. F. ATCHISON et al., "Cold Neutron Energy Dependent Production of Ultracold Neutrons in Solid Deuterium," *Phys. Rev. Lett.*, **99**, 262502 (2007); https://link.aps.org/doi/10.1103/PhysRevLett.99.262502.
42. A. FREI et al., "Understanding of Ultra-Cold–Neutron Production in Solid Deuterium," *Europhys. Lett.*, **92**, *6*, 62001 (2011); https://doi.org/10.1209/0295-5075/92/62001.
43. C. Y. LIU et al., "Coherent Neutron Scattering in Polycrystalline Deuterium and Its Implications for Ultracold Neutron Production" (2010); https://arxiv.org/abs/1005.1016.
44. A. SEREBROV and V. LYAMKIN, "Development of UCN Sources at PNPI," *Proc. Workshop Very Cold and Ultra Cold Neutron Sources for ESS*, Virtual Workshop, February 2–4, 2022.
45. O. ZIMMER, "In-Beam Superfluid-Helium Ultracold-Neutron Source for the ESS," *Proc. Workshop Very Cold and Ultra Cold Neutron Sources for ESS*, Virtual Workshop, February 2–4, 2022.
46. O. ZIMMER, "Imaging Nested-Mirror Assemblies—A New Generation of Neutron Delivery Systems?" *J. Neutron Res.*, **20**, *4*, 91 (2019); https://doi.org/10.3233/JNR-190101.
47. X.-X. CAI and T. KITTELMANN, "NCrystal: A Library for Thermal Neutron Transport," *Comput. Phys. Commun.*, **246**, 106851 (2020); https://doi.org/10.1016/j.cpc.2019.07.015.
48. ncplugin-SANSND website; https://github.com/highness-eu/ncplugin-SANSND/.
49. V. V. NESVIZHEVSKY et al., "Effect of Nanodiamond Fluorination on the Efficiency of Quasispecular Reflection of Cold Neutrons," *Phys. Rev. A*, **97**, *2*, 023629 (2018); https://link.aps.org/doi/10.1103/PhysRevA.97.023629.
50. M. JAMALIPOUR et al., "Improved Beam Extraction at Compact Neutron Sources Using Diamonds Nanoparticles and Supermirrors," *EPJ Web Conf.*, **1033**, 166719 (2022); https://www.sciencedirect.com/science/article/pii/S0168900222002510.
51. R. CUBITT et al., "Quasi-Specular Reflection of Cold Neutrons from Nano-Dispersed Media at Above-Critical Angles," *Nucl. Instrum. Methods Phys. Res., Sect. A*, **622**, *1*, 182 (2010); http://www.sciencedirect.com/science/article/pii/S0168900210016591.
52. L. ROSTA, Personal Communication (2022).
53. M. BERTELSEN, "The Automatic Neutron Guide Optimizer Guide_bot," *Nucl. Instrum. Methods Phys. Res., Sect. A*, **867**, 195 (2017); https://doi.org/10.1016/j.nima.2017.06.012.
54. D. MILDNER and M. GUBAREV, "Wolter Optics for Neutron Focusing," *Nucl. Instrum. Methods Phys. Res., Sect. A*, **634**, *1*, S7 (2011); https://doi.org/10.1016/j.nima.2010.06.093.
55. D. LIU et al., "Demonstration of a Novel Focusing Small-Angle Neutron Scattering Instrument Equipped with Axisymmetric Mirrors," *Nat. Commun.*, **4**, *1*, 1 (2013); https://doi.org/10.1038/ncomms3556.
56. M. ABIR, D. S. HUSSEY, and B. KHAYKOVICH, "Design of Neutron Microscopes Equipped with Wolter Mirror Condenser and Objective Optics for High-Fidelity Imaging and Beam Transport," *J. Imaging*, **6**, *10*, 100 (2020); https://doi.org/10.3390/jimaging6100100.
57. A. LAPINAITE, T. CARLOMAGNO, and F. GABEL, "Small-Angle Neutron Scattering of RNA–Protein Complexes," *RNA Spectroscopy*, p. 165, Springer.
58. T. REIMANN et al., "Visualizing the Morphology of Vortex Lattice Domains in a Bulk Type-II Superconductor," *Nat. Commun.*, **6**, *1*, 1 (2015); https://doi.org/10.1038/ncomms9813.
59. S. MÜHLBAUER et al., "Magnetic Small-Angle Neutron Scattering," *Rev. Mod. Phys.*, **91**, *1*, 015004 (2019); https://doi.org/10.1103/RevModPhys.91.015004.
60. C. GLINKA et al., "Sub-Millisecond Time-Resolved Small-Angle Neutron Scattering Measurements at NIST," *J. Appl. Crystallogr.*, **53**, *3*, 598 (2020); https://doi.org/10.1107/S1600576720004367.
61. H. WOLTER, "Spiegelsysteme Streifenden Einfalls als abbildende Optiken für Röntgenstrahlen," *Ann. Phys.*, **445**, *1–2*, 94 (1952); https://doi.org/10.1002/andp.19524450108.
62. T. KITTELMANN et al., "Monte Carlo Particle Lists: MCPL," *Comput. Phys. Commun.*, **218**, 17 (2017); https://www.sciencedirect.com/science/article/pii/S0010465517301261.
63. K. H. ANDERSEN et al., "The Instrument Suite of the European Spallation Source," *Nucl. Instrum. Methods*

Phys. Res., Sect. A, **957**, 163402 (2020); https://doi.org/10.1016/j.nima.2020.163402.

64. M. BALDO-CEOLIN et al., "A New Experimental Limit on Neutron-Antineutron Oscillations," *Z. Phys. C*, **63**, *3*, 409 (1994); https://doi.org/10.1007/BF01580321.
65. O. ZIMMER, "Multi-Mirror Imaging Optics for Low-Loss Transport of Divergent Neutron Beams and Tailored Wavelength Spectra," arXiv:1611.07353 [hep-ex, physics: nucl-ex,physics: physics] (2016).
66. E. ABBE HON, "VII.—On the Estimation of Aperture in the Microscope," *J. R. Microsc. Soc.*, **1**, *3*, 388 (1881); https://onlinelibrary.wiley.com/doi/abs/10.1111/j.1365-2818.1881.tb05909.x.
67. S. ANSELL, "CombLayer—A Fast Parametric MCNP(X) Model Constructor," *Proc. 21st Mtg. International Collaboration on Advanced Neutron Sources*, Mito, Japan, September 29–October 3, 2014 (2015); https://doi.org/10.11484/jaea-conf-2015-002.
68. J. GOORLEY et al., "Initial MCNP6 Release Overview," LA-UR-13-22934, Los Alamos National Laboratory (2013).
69. K. ANDERSEN et al., "The Instrument Suite of the European Spallation Source," *Nucl. Instrum. Methods Phys. Res., Sect. A*, **957**, 163402 (2020); https://www.sciencedirect.com/science/article/pii/S0168900220300097.
70. M. HOLL et al., "Beamline Simulation for the NNBAR Experiment at the European Spallation Source" (2022); https://arxiv.org/abs/2209.08997.
71. S.-C. YIU et al., "Status of the Design of an Annihilation Detector to Observe Neutron-Antineutron Conversions at the European Spallation Source," *Symmetry*, **14**, *1*, 76 (2022); https://doi.org/10.3390/sym14010076.
72. J. BARROW et al., "Computing and Detector Simulation Framework for the HIBEAM/NNBAR Experimental Program at the ESS," *EPJ Web Conf.*, **251**, 02062 (2021); https://doi.org/10.1051/epjconf/202125102062.